CHALMERS
UNIVERSITY OF TECHNOLOGY

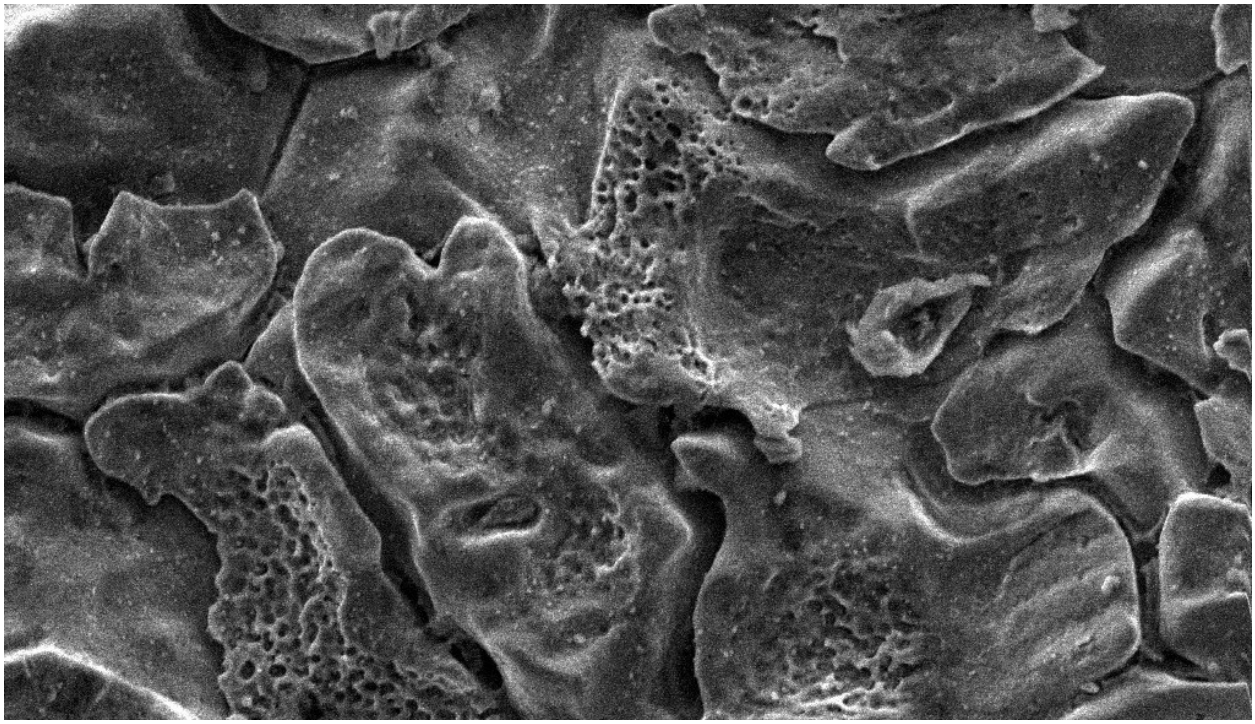

Novel Nanomaterial Surface Treatments within Subsea Processing

An investigation of a novel surface treatment, analyzing its capability to improve subsea cooling

Master's thesis in Materials Chemistry

ELIN FORSLING & JONATHAN HAGLUND

DEPARTMENT OF CHEMISTRY AND CHEMICAL ENGINEERING

CHALMERS UNIVERSITY OF TECHNOLOGY
Gothenburg, Sweden 2023
www.chalmers.se

Master's thesis 2023

Nanomaterial Surface Treatments within Subsea Processing

An investigation of a novel surface treatment, analyzing its capability to improve subsea cooling

ELIN FORSLING
JONATHAN HAGLUND

CHALMERS
UNIVERSITY OF TECHNOLOGY

Department of Applied Chemistry
Division of Chemistry and Chemical Engineering
Chalmers University of Technology
Gothenburg, Sweden 2023

Nanomaterial Surface Treatments within Subsea Processing
An investigation of a novel surface treatment, analyzing its capability to improve subsea cooling
ELIN FORSLING
JONATHAN HAGLUND

Supervisor: Anton Riström, Aker Solutions
Supervisor: Corinne Rostaing-Tayard, Aker Solutions
Examiner: Andreas Dahlin, Division of Applied Chemistry

Master's Thesis 2023
Department of Chemistry and Chemical Engineering
Division of Applied Chemistry
Chalmers University of Technology
SE-412 96 Gothenburg
Telephone +46 31 772 1000

Cover: Nanomaterial Surface Treatment visualized in SEM.

Typeset in LaTeX
Printed by Chalmers Reproservice
Gothenburg, Sweden 2023

Nanomaterial Surface Treatments within Subsea Processing
An investigation of a novel surface treatment, analyzing its capability to improve subsea cooling
ELIN FORSLING
JONATHAN HAGLUND
Department of Chemistry and Chemical Engineering
Chalmers University of Technology

Abstract

Sustainability is of great importance to maintain humanities quality of life as well as preserving natural resources for future generations. The strive towards sustainability promotes innovation, causing industries and their equipment to become more effective than ever before. Aker Solutions, a company within the energy sector, have several projects focusing on sustainability and increasing efficiency, one of which is improving upon the subsea cooling systems. In this project a *novelty surface treatment* was investigated and proven to challenge conventional materials, otherwise used in subsea cooling and processing. The surface treatment is based on *Yttrium nanoparticles* which affects the surface morphology of the metal utilizing the *reactive element effect*, ultimately increasing the surface's *corrosion resistance* and *fouling mitigation* properties. Three different variations of the surface treatment on five different Iron, or Nickel based alloys were evaluated along with the bare alloys and other commonly used materials. Counting up to 19 material systems in total. Since the surface free energy has been found to affect fouling and microbial growth, contact angle measurements and calculations in line with the OWRK method generated each material system's total surface free energy and its polar and dispersive contribution. It was from these measurements proven that the polar contribution of the surface free energy is eliminated post surface treatment, however it was the fouling test which determined the superiority of a specific surface treatment variation, from both its resistance to corrosion and fouling mitigation properties. This particular version of the surface treatment was thermally treated for relatively longer period at a lower temperature, causing the protective oxide formed to become thicker or denser, thus less oxygen permeable. Due to the minimal amount of Yttrium added to the surface of the otherwise common material the CAPEX is relatively low. Additionally, the surface treatment has potential of superior operational lifetime as well as being a more environmentally conscious choice.

Keywords: Corrosion, Fouling, Nanomaterials, Subsea Cooling, Surface Treatments

Acknowledgements

We are sincerely grateful for all support, both professionally and financially, we have got from Aker Solutions to be able to perform this work. We are specially thankful for Corinne Rostaying-Tayard for her inputs and guidance throughout the project and for Anton Riström and Henrik Alfredsson, who has made sure we were provided with all necessary needs to perform all the tests and analyses thorughout the project to pursue the final results.

We would also like to thank Andreas Dahlin and John Andersson for providing us with the opportunity to conduct our research at Chalmers Division of Applied Chemistry and for all of the resources and support they provided.

We are tremendously grateful to Ph.D Susan Kerber at Material Interface Inc. for the opportunity to investigate Susan's product and to learn from her knowledge about the material technology. Additionally, Jonathan sends his greatest appreciations to Susan for her kindness and hospitality during his visiting to Wisconsin.

Last, but not least, we would like to thank our families and friends for all the loving support throughout our entire academical careers. Without the emotional encouragement they have provided us with, our journeys would not have been possible.

Elin Forsling and Jonathan Haglund, Gothenburg, June 2023

List of Abbreviations and Acronyms

Below is the list of abbreviations and acronyms that have been used throughout this thesis listed in alphabetical order:

CAPEX	Capital Expenditure
DMSO	Dimethyl Sulfoxide
EDX	Energy Dispersive X-Ray Spectroscopy
EWF	Electron Work Function
MIC	Microbial Induced Corrosion
OPEX	Operational Expenditure
PTFE	Polytetraflourethylene
REE	Reactive Element Effect
SEM	Scanning Electron Microscopy
SFE	Surface Free Energy
SHP	Standard Hydrogen Potential
TBC	Thermal Barrier Coating
TGO	Thermally Grown Oxide

Nomenclature

Below is the nomenclature of indices, sets, parameters, and variables that have been used throughout this thesis.

Indices

P	Polar
D	Dispersive
s	Solid
l	Liquid
v	Vapour
f	Fouling

Parameters

Φ	Electron Work Function
V_e	Vacuum Energy Level
E_F	Fermi Energy Level
χ	Chemical Contribution to the EWF
Ψ	Electrical Contribution to the EWF
γ_{sv}	Surface Free Energy of the Solid
γ_t	Surface Tension for the Liquid
γ_{lv}^D	Dispersive Part of the Liquids Surface Tension
γ_{lv}^P	Polar Part of the Liquids Surface Tension
γ_{sv}^D	Dispersive Contribution to the SFE
γ_{sv}^P	Polar Contribution to the SFE
θ	Contact Angle between Material Surface and Liquid
m_0	Mass of Filter Paper before Fouling were added

m_f	Mass of Fouling
A_f	Surface Area where the Fouling were examined
ξ	Fouling in g/cm^2
U_f	Fouling Factor

Contents

List of Figures

List of Tables

1
Introduction

In this chapter, the main target of the project is going to be introduced along with certain aspects regarding the applications of technical materials in subsea environments. The main focus of the investigation is the way properties, for certain materials, can ensure stable processes in *subsea environment*. Alas, which materials are best to use for circumstances present in underwater conditions without facing issues due to the operating environment and why. Generally, for subsea applications, the largest risks is oxidation of the metal and a mass loss due to *corrosion* as well as other major aspect within *marine fouling*.

1.1 Background

Human society and industries today require a wast amount of energy to function. Historically, tools, facilities and machines were built making labour more efficient but society was yet dependent on human efforts, as a source of energy. Then, coal and electricity was a big part of the industrialization. Further, when oil and gas was discovered during the 19th century it revolutionized the efficiency of the energy sector. [1, 2] The current situation however pushes the energy sector to become more sustainable. That is, minimizing emissions, improving efficiency, and replacing fossil fuels. Aker Solutions is a Norwegian company, one of many companies working within the energy sector, and Norwegian energy companies in general have a long history within the gas and oil industry. Within this industry, sustainability is an important topic and a lot of Aker Solutions' upcoming projects are in, for instance, the zero emission category. One of the main projects according to the zero-emission aim for Aker Solutions is the so called *Offshore Wind Platforms*, where wind power stations are located offshore around the globe. By using offshore wind power stations, the wind is more likely to be even and more frequent than onshore. It is also beneficial for the shoreline environment and wildlife to use the power stations offshore. [3]

There are a lot of benefits with using the sea as a place for energy production. Most of the equipment is located subsea which makes the cooling procedure of the media inside the pipes natural. In subsea coolers, the seawater temperature is cooling the system, and depending on the desired temperature and the inlet temperature the cooler is designed differently.[4] A system with a high inlet temperature and a low desired temperature requires more cooling loops, causing the amount of cooling loops to be highly dependent on the dT. This could scale up the size of a subsea cooler drastically and one of the aims with this project is to impede this sizing problem.

Stainless steels are widely used in offshore and subsea engineering due to its resistance to localized corrosion attacks along with its high strength. But as the engineering community is moving forward, new and more requirements are introduced and ordinary stainless steels are no longer the optimal solution. Nowadays, subsea compression stations are planned to operate for several decades without any maintenance, causing the material requirements to be way more comprehensive. Fouling and corrosion is the main point of investigation when developing new material systems able to fulfil these requirements. The product of fouling causes the heat transfer between heating and cooling media to become less effective. This compels the instrumentation to allow for losses, in turn urging the heat exchanger in question to require larger heat transfer area. By minimizing the ability of this fouling phenomenon to occur during operation, the sizing of the coolers could be minimized without jeopardizing the efficiency of the cooler. The novelty surface treatment which is to be assessed in this study has shown to lower the surface free energy of the base material extensively. Based on the knowledge of low surface free energy being connected with inhibiting marine growth [5], the expectation is to observe improved fouling mitigating properties and corrosion resistance of the treated samples, due to reduced microbially induces corrosion, MIC.

1.2 Aim

Collecting and analyzing data on the chosen alloys and coatings will generate improved knowledge about what kinds of material systems are preferred to use in subsea environments. This data will essentially be linking fouling and corrosion resistance to properties related to material system's surface chemistry. Furthermore, the data collected will additionally be a part of the basis to support construction choices of Aker Solutions. This forms the collective aim to increase efficiency within industrial processing. In particular, increase efficiency by decreasing losses due to insufficient heat transfer and increase the service life of subsea heat exchangers. Eventually, giving rise to a more sustainable social, environmental and economic future within the energy sector. The aim of the project is to investigate a novelty surface treatment and its effect within different material systems, evaluating varieties in both the treatment method as well as the treated metal alloy. Additionally, by analysing material systems, commonly used in subsea processing, achieving comparative results; establishing a connection between academia and industrial common practice.

1.3 Problem description

Since energy generation is accountable for both emissions and general safety risks, there is a constant strive for improvement. The environmental aspects push technology towards innovation, while safety concerns require a more conservative perspective. Subsea environment is harsh and can rapidly degrade and compromise structures which otherwise are accepted for onshore processing. The material system has to be both corrosion and fouling resistant, while clearly also suitable for the intended application. An important material property for heat exchangers is the *thermal conductivity* or k-value. Common materials used currently can however be improved or should to be replaced. Some materials, like stainless or duplex steels, have superior corrosion resistance and acceptable thermal conductivity but are susceptible to fouling in subsea environment. Standard copper alloys have extraordinary antifouling properties and corrosion resistance, good thermal conductivity, but are inherently toxic and expensive. To improve surface properties the base material can be coated, although coatings bring forth aspects regarding adhesion and added thickness, ultimately affecting the heat transfer. Additionally, the lifetime of structures is desired to increase while cutting the amount of maintenance. This, along with harsh subsea environment, implies tough requirements regarding the choice of structures' materials. A novel surface treatment using nanoparticles of Yttrium is believed to have the ability to improve both fouling and corrosion resistivity. Whether this is the case will be investigated in this project.

2
Theory

This chapter provides the theory on which this project is based. The information stated ranges from physical, chemical and environmental phenomena to specific details about the materials, coatings and treatments used, and also extensively explaining the theoretical framework of the project. The first Sections, 2.1 to 2.2, contains relevant information to understand inherent phenomena of the novelty nanomaterial surface treatment. Furthermore, theories regarding surface free energy followed by marine fouling and corrosion, which are key topics within this project. Integrated knowledge of material and surface properties which could affect subsea processing are also being demonstrated. Lastly, the materials examined in the project are introduced. Accounting for both specifics and applications of the materials. The materials are in this projects subdivided into alloys and coatings.

Integrated knowledge of material and surface properties which could affect subsea processing are also being demonstrated

2.1 Rare Earth Elements

The *Rare Earth Elements* is a group of elements in the periodic table, located in period 3, including atomic numbers *21, 39* and the *lanthanides, 57-71*, shown in Figure 2.1. [6]

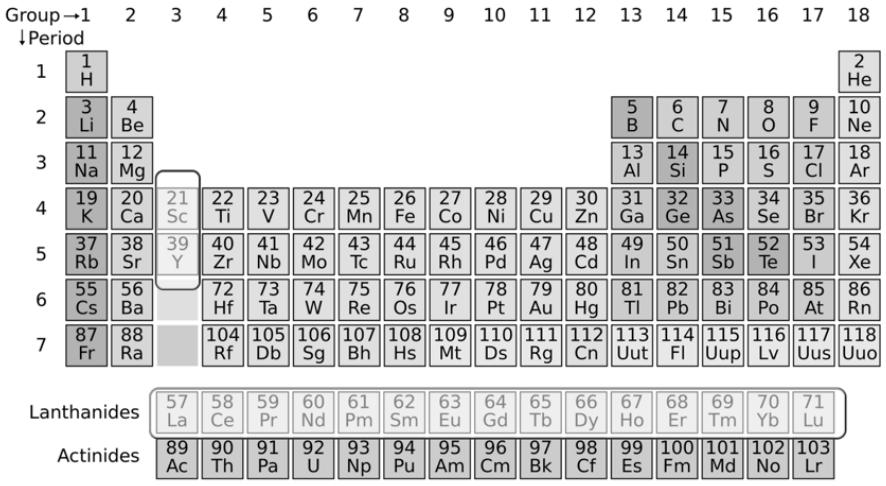

Figure 2.1: The Periodic Table of Elements. Rare Earth Elements are highlighted in period 3.

The discovery of *Rare Earth Elements* were made at the end of the 18th century by the Finnish chemist Johann Gadolin in Ytterby, a small island in the Stockholm archipelago. The element that was found, Yttrium, Y, was suitably named after the discovery location. [6] Yttrium is a key element in this project due to its *Rare Element Effect* (2.1.1) properties, affecting the surface treatment of interest.

The definition *Rare* Earth Elements is quite misleading, since the occurrence of these elements are quite common in the nature around the world, but most commonly found in China, which is the only producer of heavy rare earth elements, and the U.S. Although the origin of rare earth elements is in Scandinavia. [7]

Furthermore, rare earth elements do not occur frequently in concentrations high enough for it to be economically beneficial to mine the material. Another risk that has to be taken into consideration is the number of workable rare earth deposits, which are being limited by the geochemical properties of these minerals. The ore materials of rare earth elements are very seldom pure enough to mine directly. An example of this issue is the mineral *monazite*, $(Ce, La, Th)PO_4$. [8] Further investigation of (Th)-monazite, $ThPO_4$, and accumulation during processing of the mined ore could introduce so called 'daughter products' of the original Rare Earth Element based mineral. Even though Thorium is not a very radioactive material per se, production and processing of Thorium may result in exposure and production of radioactive actinides such as Uranium, U, and the commonly known element, Radium, Ra. [8]

2.1.1 Reactive Element Effect

Rare elements, such as the Lanthanides, Scandium and Yttrium has proven to be beneficial to add, in a very small amount, to metallic alloys to significantly improve its mechanical and physical properties. The rare elements are also able to modify the crystal structure and hence improve the alloys resistancy to corrosion and high temperature oxidation. [9] In general, when passivating materials to achieve an increased oxidation resistance, alloys like stainless steels, Chromium induced Nickel alloys or $Ni-Al$ bronzes experiencing great protective properties upon passivation to form Al_2O_3 and Cr_2O_3 respectively. These oxides are the most common protective oxides and can be compared to a protective coating of a metal surface. These oxide layers are experiencing lower surface energies than the bare metal surfaces and furthermore increase the hydrophobicity of the surface enhancing the anti fouling properties of the investigated metal sample. [10]

The oxidation process in a metal in harsh environments is an outward diffusion process from the alloy out towards the surface, where the corresponding metal oxides are formed. These oxides are caused by oxidation of the metal and could be placed in the corrosion category of oxidation. By adding rare earth elements to the alloy, which is more oxygen reactive than scale forming, the diffusion direction is being reversed, meaning that the surface particles rather reacting with the surrounding oxygen than with particles from the bulk. [11] When adding rare earth elements to the alloy in a very small amount, the rare earth elements tend to stay on the surface, causing oxygen to diffuse through the layer of rare earth oxides, through the surface and towards the bulk. The oxide formed on the surface could be categorized as a nanooxide layer consisting of chromium rich oxides, Cr_2O_3 and rare earth oxides, RE_2O_3. [12] The particles in this nanooxide are in the nanoscale regarding its size, causing the oxygen to no longer be able to diffuse through the nanoscale grains on the surface, and hence the oxide growth on top of the rare earth oxide is strongly restricted. [13] A decreased amount of oxide growth on top of the rare earth oxide is furthermore implementing a strong decrease in the corrosion rate for the metal because of the interruption in the galvanic reaction.

2.2 Electron Work Function

The electron work function, Φ, often denoted as EWF, is the minimum amount of energy required to remove an electron from a solid surface in the *Fermi Level* to a point immediately outside the surface, often called the *Vacuum Energy Level*. The EWF could furthermore be expressed as Equation 2.1: [14]

$$\Phi = V_e - E_F \tag{2.1}$$

A material with low work function is more likely to act as an electron donor than a material with high work function. [15] The EWF is a very important theory regarding photoelectrical applications, but could also be applicable in surface engineering regarding the contribution to the charges on the materials surface. The work function could be devided into its chemical (χ) and electrical (Ψ) contribution

and hence, the summation of these ends up in the total work function as described in Equation 2.2:

$$\Phi = \chi + \Psi \tag{2.2}$$

The chemical contribution is based on the correlation and exchange energy of a given Fermi Level and applies on the bulk level of the material, while the elecrical contribution is dependent on both the chemical contribution along with surface properties. The electrical charges are furthermore redistributing themselves on the surface of the material, causing the charge distribution to vary depending on which element that is being added to the surface. [16] In Table 2.1, a few interesting electron work function values is displayed [17].

Element	Φ [eV]	**Plane**
Al	4,20	(100)
Cr	4,50	Polycrystalline
Cu	5,10	(100)
Fe	4,67	(100)
Ni	5,22	(100)
Y	3,10	Polycrystalline

Table 2.1: Electron Work Function for investigated elements. The investigated planes are all (100) except for the polycrystalline samples. The EWF has been calculated with the photoelectric effect.

In general, the pure metallic particles experience a higher EWF than its oxide based counterpart, but some oxides do experience lower EWF than its metallic counterpart. Yttrium and Yttrium oxide are one of those. An example important to this study is a comparison to Chromium along with its oxide counterpart with how the EWF changes for Yttrium upon oxidation. [13]

Substance	Φ [eV]
Metallic Yttrium	3,10
Yttria	2,00
Metallic Chromium	4,50
Chromia	5,0

Table 2.2: Electron Work Function for Yttrium, Chromium and there oxide counterparts.

2.3 Surface Free Energy

Imagine a liquid drop on a flat surface, as demonstrated in Figure 2.2. The surface tension of the solid-vapour surface interface, γ_{sv}, also known as the *Surface Free Energy*, SFE, can be described using the surface tension of the liquid-vapour interface, γ_{lv}, and the surface tension of the solid-liquid interface, γ_{sl}. Surface tension plays a

direct role in liquid spreading on a solid surface, or *wetting*. Poor liquid spreading and a low SFE is indicated by a larger *contact angle*, CA, illustrated as θ in Figure 2.2. [18]

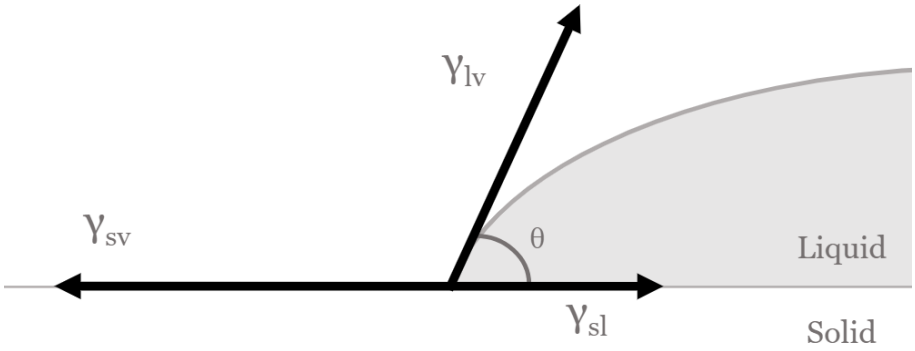

Figure 2.2: Liquid spreading on solid surface, including the surface forces involved and the contact angle, θ.

The phenomenen of a drop's spreading on solid surfaces was first formulated by the words of Thomas Young. Generally known as Young's equation, Equation 2.3 describes the relation between the forces acting on the drop and the CA.[18]

$$\gamma_{sv} = \gamma_{sl} + \gamma_{lv} cos\theta \tag{2.3}$$

2.3.1 Polar and Dispersive Surface Energies

The surface free energy can be devided into two different parts depending on the forces being active on a materials surface, the polar and the dispersive contributions of the SFE. The polar contribution is due to electron asymmetry on the substrates surface and is driven by permanent or localized dipole moments, where some molecules and surfaces have structural properties which enhance the creation of permanent dipole moments. These permanent dipole moments are furthermore increasing the charge distribution on the material surface and hence promoting polar forces on the surface. [19] Dispersive surface energies, on the other hand, are based on fluctuations in the electron density present in molecules on the material surface. These forces corresponds to London forces and are weak in comparasion to polar forces. The dispersive contribution is also a measurement for the abilty to form van der Waals interactions with other materials. [20]

2.3.2 The OWRK Method

To be able to decide the polar and dispersive parts of the surface energy of the material systems being investigated, and to eventually draw parallel's between fouling and certain surface properties, the OWRK method for surface energy measurements has been used.

The OWRK method has been named after four chemists, *Owens, Wendt, Rabel and Kaelble*. These made it possible to decide the ratio between the dispesive and

polar surface energy of any specimen by using two, or more, different liquids with known dispersive and polar parts of the surface tension. The solid-liquid interface tension could furthermore be expressed by Equation 2.4 below. [21, 22]

$$\gamma_{sl} = \gamma_{sv} + \gamma_{lv} - 2\left(\sqrt{\gamma_{sv}^{D}\gamma_{lv}^{D}} + \sqrt{\gamma_{sv}^{P}\gamma_{lv}^{P}}\right) \tag{2.4}$$

Further derivation of the expression is needed to clarify the equation and to determine the total surface energy of the surface investigated. Combining Equation 2.3 and Equation 2.4 presented below:

$$\gamma_{sv} = \gamma_{sl} + \gamma_{lv}cos\theta \longleftrightarrow \gamma_{sl} = \gamma_{sv} - \gamma_{lv}cos\theta$$

Inserting γ_{sl} in Equation 2.4 and rearranging the equation, formulates Equation 2.5.

$$\sqrt{\gamma_{sv}^{D}\gamma_{lv}^{D}} + \sqrt{\gamma_{sv}^{P}\gamma_{lv}^{P}} = \frac{1}{2}\Big[\gamma_{lv}(1 + cos\theta)\Big] \tag{2.5}$$

The Equation 2.5 is subsequently used to decide the polar and dispersive part of the SFE. Nevertheless, to calculate the polar and dispersive parts, a system of two equations with two unknowns needs to be solved for using two liquids with known liquid-vapour interfacial tensions and their polar and dispersive contributions to their surface tensions, Equations 2.6. The use of the demarcation 1, or 2, signifies these two different liquids used, where it is suitable to use the least polar liquid as liquid 1.

$$\begin{cases} \gamma_{sv}^{D} = \dfrac{\left(\frac{1}{2}\Big[\gamma_{lv,1}(1 + \cos\theta_1)\Big] - \sqrt{\gamma_{sv}^{P}\gamma_{lv,1}^{P}}\right)^2}{\gamma_{lv,1}^{D}} \\ \gamma_{sv}^{P} = \dfrac{\left(\frac{1}{2}\Big[\gamma_{lv,2}(1 + \cos\theta_2)\Big] - \sqrt{\gamma_{sv}^{D}\gamma_{lv,2}^{D}}\right)^2}{\gamma_{lv,2}^{P}} \end{cases} \tag{2.6}$$

Further simplifying and setting the right hand side of the equation to zero is displayed in 2.7:

$$\begin{cases} \gamma_{sv}^{D} - \dfrac{\left(\frac{1}{2}\Big[\gamma_{lv,1}(1 + \cos\theta_1)\Big] - \sqrt{\gamma_{sv}^{P}\gamma_{lv,1}^{P}}\right)^2}{\gamma_{lv,1}^{D}} = 0 \\ \gamma_{sv}^{P} - \dfrac{\left(\frac{1}{2}\Big[\gamma_{lv,2}(1 + \cos\theta_2)\Big] - \sqrt{\gamma_{sv}^{D}\gamma_{lv,2}^{D}}\right)^2}{\gamma_{lv,2}^{P}} = 0 \end{cases} \tag{2.7}$$

Hence, the total SFE is calculated easily with the following expression, i.e. the summation of the dispersive and the polar part of the SFE.

$$\gamma_{sv} = \gamma_{sv}^{P} + \gamma_{sv}^{D} \tag{2.8}$$

Listed in Table 2.3, below, are the explanations for the certain parameters used in equations 2.3-2.7.

Table 2.3: Explanations of variables.

Value	Variable
Total Surface Tension for the liquid	γ_l
Dispersive part of Surface Tension for the liquid	γ_{lv}^D
Polar part of the Surface Tension for the liquid	γ_{lv}^P
Dispersive part of the SFE	γ_{sv}^D
Polar part of the SFE	γ_{sv}^P
Mean value of the Contact Angle	θ

2.4 Marine Fouling and Antifouling Technologies

Marine fouling or *biofouling* is the phenomenon of micro- and macro-organisms adhering and accumulating on a submerged surface. Generally it is associated with negative environmental, safety, and economic effects, and it is an established problem in the both seafaring and other industries. Marine fouling causes deterioration of coatings, in turn, leading to an increased corrosion rate, as well as counteracts conductive heat transfer by increasing the heat transfer resistance. [23, 24]

When submerging a metal structure, the metal surface is exposed to both liquid and its accompanying bacteria, microorganisms. Consequently, some bacteria attach to the surface causing subsequent adhesion of additional bacteria, eventually covering the metal surface in a *biofilm.*[25, 26] The variation of microbial life is extensive and it thrives as long as water is present. Microbial growth can be found in environments with temperatures ranging from -10 to 114 °C and pressures up 1 000 bar. [27] However, there are some requirements other than the presence of bacteria to generate a biofilm. Both nutrients and liquid water must be present. Since water evaporates at higher temperatures, the biofilms are more abundant in cooling towers than turbines, for instance. [28] Water at lower temperature reduces the hydrophobicity of the bacterial cell surface causing less biofilm development. Then again, low temperature also induces some functions which increase biofilm formation as well. [29] Although, the term *biofilm* is old and incorrect terminology. The biofilm is rather a structure that alternates between construction, deconstruction and re-construction, that is creating patchiness which is believed to ultimately accelerate the corrosion rate by allowing for a varied electrochemical concentration. [28]

It is established that bacterial development depends on SFE, surface roughness and the velocity of the surrounding fluid. Surfaces with low initial SFE generally have less long-term adhesion of biological systems. This is partly due to how the biofilm forms on the surface. The initial step, microfouling, is when free-floating bacteria attach to a surface through Van der Waals or electrostatic forces. The bacteria is then weakly attached and can be removed mechanically. [5, 26, 30]

Prevention of biofouling on marine structures is of great historical significance and dates back to around 700 BC with the Phoenicians and Carthaginians. Literature from the Romans also suggest the extensive use of copper, lead and tar on wooden ships. Antifoulants like paints and solvents based on copper-, arsenic-, and mercury-oxide were first introduced during the end of the 18th century. By 1958

the highly toxic organotin tributyltin, TBT, was gaining popularity. TBT and its related organotin compounds later made up 70% of the antifouling paint used on the world fleet. The function of conventional antifouling paints is to diffuse near surface free associated biocides out of the paint matrix, hence releasing toxic compounds into the marine environment. [31, 32] Thus, the reason why the conventional antifouling paint works is also ultimately a cause of an environmental concern of marine systems. [33] Due to excessive use resulting in elevated ambient concentrations, the production of TBT was banned by *International Maritime Organization*, IMO, in 2008 because of its negative effect on marine environments. [31, 32] Following the global ban of TBT, the antifouling paints conventionally used were based on Cu(I) biocidal pigment. [32, 33, 34] Fortunately, eco-friendly coatings and materials are becoming of bigger interest, consequently manifesting the significance of surface morphology and chemical composition. [35]

The environmental impact of using antifouling paints are however complex. Some specific leaching paints, when applied on a structure as a coating, release toxic chemicals. Moreover, particles of coatings which have been chipped off, such as during maintenance, continue to contaminate the surrounding marine environment. Thus, both through leaching of biocidal chemicals but also as synthetic micro-debris. [36] These paint particles are sometimes referred to as *antifouling pain particles*, APP. Since the APPs have larger surface area, some trace metals leach even quicker from the APPs than from the coating itself. [33] Not all paints and coatings used are leaching, however the problem of an increased amount of microplastics in marine environments remain. The research concerning microplastics in these environments are somewhat inconsistent, that is as to whether paint particles are included in the classification microplastics. Paint particles are in this study considered as microplastics, both based on the definition of microplastics and its general ecological and health effects on marine organisms after exposure. [36]

2.5 Corrosion

Corrosion is a naturally occurring phenomenon which negatively affects a metallic material's strength and surface smoothness. Both oxidizing and reducing, redox, reactions take place, involving the presence of electronic charge. Since no external charge is supplied, the same number of electrons produced by the oxidation reaction will be used in the reducing reaction, i.e. there is *charge neutrality*. Metal ions are present on the metal's surface and the metal itself thereby acts as an electrode due to its electric potential, also known as *electrode potential*. This potential relates to the change in *Gibbs free energy* and the *standard electrode potential,* E^0 i.e. the electrode potential at unit ion activity, which is related to the Gibbs free energy change in standard state, ΔG^0, represented in Equation 2.9. A metal with more negative standard electrode potential has a higher tendency to oxidize, given that it is more negative than the standard hydrogen potential, SHP. Immersing two connected metals with different redox potential in an electrolyte makes for a complete circuit. The metal with the more negative potential gets corroded since it functions as an *anode* while the less negative potential acts as a *cathode*. This setup is generally referred to as a Galvanic cell and is the theoretical framework of sacrificial anode.

$$\Delta G^0 = -nFE^0 \tag{2.9}$$

There are different kinds of corrosion. Mentioned in this study are *general corrosion* and *localized corrosion* like *pitting* and *crevice corrosion*. The most common type of corrosion is the general or uniform corrosion which affects the surface uniformly and causing loss of material thickness hence reducing the load-baring capacity. Pitting and crevice corrosion however, are localized types of corrosion and is problematic in another sense than general corrosion. Pitting is not easily discovered since the pitting area is covered by corrosion product and is mainly apparent once liquid is released from the pit. The initiated pit is also propagating by an accelerating rate along the thickness, causing pitting to become increasingly severe. Crevice corrosion occurs where liquid media is trapped. Both pitting and creviece corrosion are causes of unexpected and premature failure. [25]

2.5.1 Microbially Induced Corrosion

Marine fouling can also cause metal surfaces to become less corrosion resistant through *microbially induced corrosion*, MIC or biocorrosion.[31] The bacterial growth, mentioned above as biofilm, is also made possible due to the availability of energy, which exists through electrochemical reactions and depends on the metal surface's ability to donate electrons for microbial metabolism. In other words, a metal which rather serves as an anode is more vulnerable to MIC. Additionally, an electron accepting reaction or cathode reaction is also required in the reduction reaction in, for instance sulfate-reducting bacteria, SRB, where sulfate serves as both a constituent of microbial growth and an electron acceptor reducing into sulfide. In some cases, nitrate similarily act as an electron acceptor and it has been showed that when comparing the change in standard Gibbs free energy, this redox reaction, providing energy for bacterial growth, is thermodynamically favourable. Ultimatly, sulfate, nitrate, etc., function as a cathode and is termed *biocathode*.[25, 26, 27, 28] Furthermore, it has been experimentally illustrated that the rate of cathodic reaction is increased in the presence of a bacterial biofilm due to biocatalysis. [26] As stated in Section 2.4, the biofilm is not actually a continuous film but rather of a patchy nature and it is argued that *pitting* will follow from the formation of a biofilm. [25, 26, 27, 28] It has been shown that after three days of carbon steel being exposed to SRB, pitting was developed. [28]

In recent years, the interest in MIC has increased, partly due to an increase in industrial cases reporting about the phenomena as well as interdisciplinary research studies in areas involving material, chemical, and life science. However, it has been proven to be quite difficult to produce cost estimations that is taking MIC into account due to deficient knowledge. [37, 38]

2.5.2 Stainless Steels in Subsea Environments

Stainless steel is one of the most commonly used materials in offshore and subsea environments due to its eminence in corrosion resistance and the high strength-to-weight ratio. Stainless steels can be devided into several categories, but one of

the most important categories for subsea and offshore applications are the austenitic stainless steels. These are the most chlorine resistant stainless steels, causing them to resist localized corrosion in Chlorine rich environments, such as offshore and subsea. [39] Another stainless steel type that is very useful in these environments are duplex steels. These are experiencing great resistance against localized corrosion such as pitting, but its high strength is increasing its resistance against stress corrosion cracking, making it suitable for harsh subsea environment over long time. [40] The main reason for the corrosion resistance of stainless steels and duplex steels are the chromium content present in the alloy structures. The steels are getting passivated upon oxygen exposure, creating a protective chromium oxide layer on the surface which is preventing the steels from further corrosion, see Figure 2.3. [41] In duplex steels, there are Molybdenum and Nitrogen present in the alloy in addition to the already high Chromium content. Molybdenum and Nitrogen helps to enhance the passivity of the Chromium oxide layer, while Nitrogen is also increasing the strength of the alloy. [42]

2.5.3 Copper Alloys in Subsea Environments

Copper and its alloys have been used in a considerable amount by humans throughout history and still remains an important material in human society. It is used in a range of different environments but has been preferred particularly for seawater applications. [43] The main reason is due to copper's property of corrosion resistance, which gets improved by alloying. However, alloying impairs the high conductivity of copper while also improving its mechanical properties like creep resistance, strength and fatigue performance. Additionally, Copper is known to be a hydrophobic metal. [44] The material is not allowed to be use in contact with foodstuff due to toxicity. Although, Copper and copper salts are used in applications taking advantage of its inherent biocidal properties. [43, 45]

Alloys commonly referred to as *cupronickels*, copper alloys with nickel content ranging from 2 to 46 %, are recognised for their resistance aqueous corrosion. Cupronickels are widely used in aqueous environments and cupronickel with 30% nickel is the most corrosion resistant, but the nickel content is typically lowered due to economic reasons. [46] It is believed that the corrosion and fouling resistance of cupronickels is due to a the formation of a protective oxide surface film when exposed to sea water. Leaching of copper depends on the film which is matured within weeks or months. Once formed and matured, the leached copper is minimal. [47, 48]

2.5.4 Nickel Alloys in Subsea Environments

The property of the alloy depends on the alloying element. Nickel-Copper alloys are primarily used operating with mild, reducing solutions, while Nickel-Molybdenum when handling strong, reducing solutions. On the other hand, Nickel-Iron-Chromium alloys are used for oxidizing media and Nickel-Chromium-Molybdenum alloys are more versatile and can be used in for all environments. Copper and Chromium both increase the corrosion resistance and because of the size of Chromium atoms, it also

functions as a strengthening agent in the Nickel alloy. [49] Both Nickel-Molybdenum and Nickel-Iron-Chromium alloys are used exstensivley in aqueous environments. [50]

2.6 Coatings and Surface Treatments

There are two very different coatings that have been investigated in this project in regards to their presence on the surface. One is a PTFE based paint coating and the other one is an Yttrium based nanocoating, which furthermore could be classified as a *nanomaterial surface treatment* rather than a coating.

2.6.1 PTFE based Coating

PTFE or Polytetrafluoroethylene is a flouropolymer and is a common lining material in industries. Although, PTFE is considered a thermoplastic the PTFE based coating used in this study is a thermosetting coating, PTFE within an epoxy resin matrix. [51] Fluoropolymer coatings are generally used for their low-friction surface and high corrosion resistance, based on the behaviour of the fluorine within the polymer. [52] The coating used degrades when exposed to a UV light-source.

2.6.2 Thermally Grown Oxide

A thermally grown oxide, TGO, has extremely low oxygen permeability and functions as an oxidation-resistant layer. The TGO has an important role in thermal barrier coatings, TBC, utilized in various applications like jet engines or pyrochemical reprocessing units. The requirements of a TGO in TBCs is slow growth, strong adhesion and non-permeability. The layer, which is below one micrometer in thickness, is also required to be stable and functional throughout long-term exposure. It is shown that the thickness of a TGO increases with, for instance, thermal exposure. The TGO within a TBC is typically α-aluminia and is formed due to the high aluminium contents of the so called bond coat. [53] Heavy lanthanides, which include Yttrium, arrange in a way similar to the behaviour of Aluminium: forming a tight seal preventing oxidation. [54]

2.6.3 Nanomaterial Surface Treatment

Previously, the rare element effect has been utilized by adding a small amount of rare earth elements into the alloy composition to achieve the properties mentioned in Section 2.1.1. Further technology development has made it possible to modify the surface by adding rare earth nanoparticles onto the surface by dip coating followed by heat treatment. The time and temperature for the heat treatment could vary from 1 hour at 350°C up to 96 hours at 1100°C depending on the aim. [13]

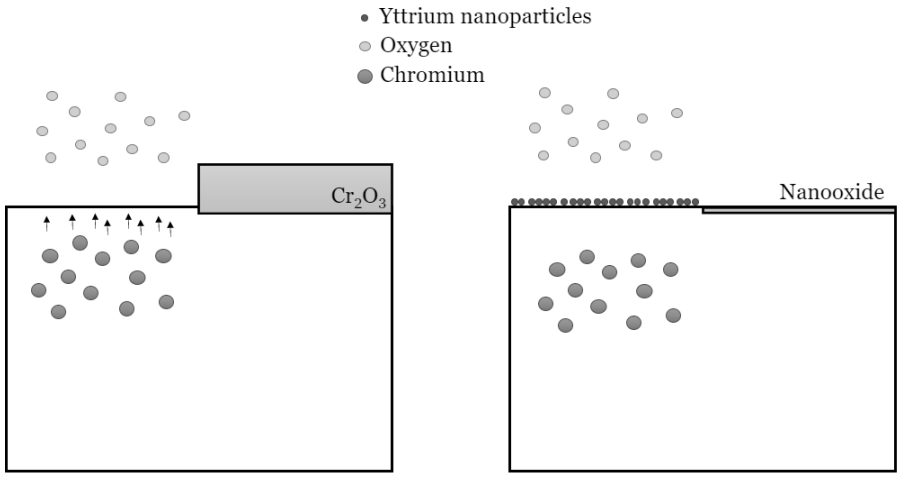

Figure 2.3: An illustation of (*left*) metal passivation of stainless steel and (*right*) formation of a nanooxide due to the nanomaterial surface treatment.

Different temperatures are providing different thermal oxides, and an increase in time is providing a thicker oxide layer. The same goes for different alloys, where certain rare earth nanoparticles modifies the the thermal oxide layer to become more stable. An example of a rare earth element with these properties is Yttrium, Y, since it is known for its strong affinity with oxygen and hence promotes the formation of Yttria, Y_2O_3. It has also been reported that the addition of Yttrium to the alloy can improve the corrosion resistance of the material by enhancing the formation of a chromium-rich oxide layer on the steel surface. [55]

The nanomaterial surface treatment consists of three major parts, which are all crucial to enhance the adhesion process of the nanoparticles. The first part is the *nanoparticles* itself, distributed all over the solution with a size of approximately $5nm$ each. Yttrium particles of this size are quite unstable and tend to lump together in the absence of a repelling force. The repelling force in this product is a *stabilizing ion*, which desorbs upon contact with air. The combination of yttrium nanoparticles and these stabilizing ions are furthermore a hydrophobic solution, unable to properly wet the metal. Hence, surfactants are added to the solution to make sure that the metal surface gets properly covered with the solution. The surfactants are furthermore evaporating when the metal surface is set to dry, and any rest products are burned away in the furnace.

3
Methodology

In this chapter, the methodologies for the different parts of the project is discussed and explained. Several measurements and tests were conducted in this project and there are essentially three categories: *Scanning Electron Microscopy* or SEM, SFE calculations and the fouling test. The project could furthermore be divided into two parts, one part is regarding laboratory work, data compilation and calculations. The second part is the fouling test which was running through the entire project time.

3.1 Laboratory Work and Data Compilation

The initial part of the project was to prepare all the coupons for the project's main part, the fouling test. This is including preparation of the coupons for the different coating treatments and the coating procedures themselves. In the meantime, when the fouling setup was submerged, additional testings to equal treated coupons were made at the Division of Applied Chemistry at Chalmers University of Technology in Gothenburg.

The main focus of these tests was to determine certain surface properties of the treated coupons, and a comparison between coated, treated and untreated materials. More specifically, the surface free energy was calculated along with its polar and dispersive contributions. Scanning Electron Microscopy analysis were further executed to investigate chemical compositions on the surface along with visual surface morphology.

3.1.1 Coupon Preparation

The coupons were provided from various metal manufacturers, and some of them were provided from Aker Solutions yard in Egersund on the Norwegian west coast. The material was provided without any treatment, and hence the cleanness of the coupons could not be guaranteed. In prior to both the nano coating and to the paint coating, a clean surface is required to ensure that the coating is properly attached to the surfaces.

The cleaning process in prior to the nanocoating was contained of two organic solvents, *acetone* and *isopropanol*, along with nitrogen gas and was conducted as a three step process. Initially, the coupons were dipped into an acetone bath and furthermore moved to an isopropanol bath.

Acetone and isopropanol are commonly used as cleaning solvents since they are very effective at dissolving a wide range of substances, including grease, oil, and dirt. Even though both of the solvents are very effective at dissolving, several steps is beneficial to the final product. Acetone is highly volatile, meaning that the evaporation time is low, so the risk of leaving residues is higher. Isopropanol is less volatile and the evaporation time is hence longer, causing the isopropanol to dissolve and remove the residues. [56] To ensure a proper evaporation of the solvents, Nitrogen gas was used to blow the coupons dry. The reason for the choice of gas is simply because Nitrogen is an inert gas free of contaminants, which might be the case for compressed air.

The coupon preparation for the PTFE based paint coating contained, except for standard cleaning procedures, grit blasting to achieve a smooth surface in prior to the paint coating procedure.

3.1.2 Coating Procedures

This project is containing investigations of two different coatings, one PTFE based paint coating, and one Yttrium based nanocoating. The deposition methods of these two is varying a lot from each other and the protectiveness does come from

very different sources. None of the coating procedures require any extraordinary environment, and both of the procedures were made in regular laboratories.

3.1.2.1 Deposition of the PTFE based Paint Coating

The PTFE based paint coating was applied though spray deposition on Alloy 1, 2, and 4. Application per the manufacturer's instructions.

3.1.2.2 Deposition of the Nanocoating

A total of 45 cleaned stainless steel coupons, 15 of each alloying grade, were brought to Material Interface Inc. in Sussex, Wisconsin, for treatment. The coating procedure are built up in three steps, where all of them are critical to achieve a good result.

- Dip coating of the coupons.
- Heat treatment for oxide growth.
- Air cooling and desorption.

An arbitrary amount of the coating solution was poured into a glass beaker, just enough to cover a coupon with the solution to ensure the entire coupon is being exposed to the nano particles. The coupons were dipped one at at time, and thereafter were set to dry on a rack. Minimal contact area between the rack and the coupons is necessary to obtain an as evenly distributed layer of nanoparticles as possible. Once the coupons were completely dry, the rack was transferred into an air vented industrial furnace.

The same procedure was repeated three times, 15 coupons each time, and three different furnace settings as following:

- Treatment 1 - Low temperature, short time
- Treatment 2 - Low temperature, long time
- Treatment 3 - High temperature, short time

The different treatment parameters producing different kinds and thicknesses of protective thermal oxides on the coupon surfaces. A visual difference between treated and non-treated coupons is furthermore shown in Figure 3.1. Depending on the treatment parameters, the coupons are going to turn into different shades. The same temperatures are providing the same kind of TGO, but a longer treatment time will enhance the formation of the TGO and hence a more dense oxide layer. A more dense oxide layer is furthermore giving rise to a darker shade of the same TGO as its short time treated counterpart due to increased density. For a treatment with higher temperature, the TGO type is changed and the shade of the oxide is therefor different.

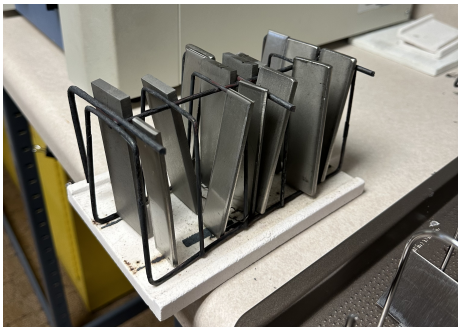

(a) Coupons before treatment

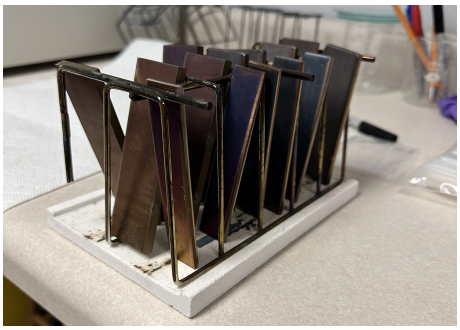

(b) Coupons treated with Treatment 3

Figure 3.1: The visual difference between pre and post heat treatment of the coupons

Once the coupons were done in the furnace, they were set to cool down in regular air environment until room temperature. The coupons were furthermore handled with clean gloves and were wrapped in degreasing wipes to be ready for transport back to Gothenburg. Upon arrival back in Gothenburg, the coupons were unwrapped and put back on a rack to let the nanoparticle stabilizing ions desorb from the coupon surface. The desorption process took approximately 48 hours to finish, and during this time the coupons were completely isolated from any interaction. Once this 48 hour of desorption time was done, the coupons were done treated.

3.1.3 Materials

Due to confidentiality of this project no specific materials or coatings will be stated direcly. All materials, coatings and surface treatments are referred as Alloy **1-7** or Coating **1-4**.

Alloy 1, 2, and 3 are all austenitic stainless steels with different alloying grades and elements. Alloy 4 is a regular carbon steel without any additional alloying elements. Table 3.1 below indices alloying grade, and certain elements in these Fe-based alloys.

Table 3.1: Alloy content - Stainless steels

Alloy No.	Main Alloying Element	Alloying Grade
1	Chromium	High
2	Chromium	Medium
3	Chromium	Medium-High
4	Carbon	Low

Alloys 5-7 does not categorize in the same category as the steel alloys, and could be further divided as in Table 3.2.

Table 3.2: Alloy content - Other alloys

Alloy No.	Main Element	Main Alloying Element	Alloying Grade
5	Copper	Nickel	Low
6	Nickel	Chromium, Copper	High
7	Nickel	Chromium, Molybdenum	Medium

Prices of the materials are somewhat linked to their relative abundance, see Table 3.3, which both play a part in the final choice of material used. [57] The unit *troy ounce*, ozt, is a measurement used for precious metal weight and is the equivalent of 31,103 g. Important to consider is that the prices listed are highly dependent on national social and economic conditions. Additionally, the prices listed do not reflect current prices and is mainly intended to be used comparatively. [57, 58, 59]

Table 3.3: Indicative prices of metals in USD per troy ounce, converted from USD per metric ton or kilogram and based on midyear market conditions of 2014. Price of Chromium and Iron is from 2016 while the price of Yttrium is from 2017.

Metal	Price [$/ozt]	Relative Abundance[a]
Aluminium	0.06	3^{rd}
Chromium	0.24	-
Copper	0.22	26^{th}
Iron	0.0026	-
Nickel	0.60	24^{th}
Tin	0.70	49^{th}
Yttrium	1.09	-

[a] Out of 78 elements, only considering elements which are found in appreciable quantities.

3.1.4 Coating systems

There are four different coating systems investigated in this project, where all are covered by confidentiality. In this subsection, the public information of the coating systems 1-4 are displayed. Coating systems 1-3 are not regular coatings, these are applied as a coating, but the final product are the interaction between the Yttrium nanoparticles and the Chromium TGO creating the Yttrium induced protective oxide. Hence, the product of the nanomaterial based soulution is a *Surface Treatment*. All of these coating systems are named as coatings to clarify that this is something added to the surface of the coupons, even though some of these are not coatings per se. Below, as detailed information as possible without jeapordizing the confidentiallity of the products, are demonstrated. The time and temperatures are confidential, but the short time treatment is at least an hour and the long time treatment does not exceed 6 hours. When discussing the temperatures of heat treatment, a temperature of at least 350° needs to be reached within the furnace to make sure the TGO is growing, according to the founder and producer of the product.

Coating 4 is PTFE-based, a coating with PTFE in an epoxy resin matrix. The coating was applied as per manufacturer's instructions at an Aker Solutions production site.

3.1.5 SEM

Further analysis of the stainless steel coupons were made in a scanning electron microscope, specifically a *FEI Quanta 200 ESEM*. The aim was to determine the density of the nanoparticle oxides and protective oxides on the rare earth element treated coupons compared to its untreated counterpart, but also to visualize the difference in chemical composition according to the morphology on different parts of the coupons. The morphology is of high importance to understand where on the coupon that fouling could be expected or not, but also how well the nanoparticles adheres to the metal surface. The nanoparticles is preferring small crevices rather than a polished surface.

Initiation of the SEM analysis were made in prior to surface treatment of the three stainless steels being investigated in the project. They were analyzed one at the time, and the surface morphology were investigated visually by back-scattered electrons at 20 kV for all of the untreated coupons, in order to see the rare earth nanoparticles the electron voltage was decreased to 10 kV. The coupons were investigated on both the cutting edges and the metallic surfaces in five different magnifications, 500x, 1000x, 2000x, 5000x and 10000x on the same place on the coupon.

The coupons were furthermore analyzed in the EDX detector to analyze the surfaces chemical compositions. Primarily to investigate whether any oxides were present on the coupon surface in prior to the coating treatment, and the chemical compositions of the protective oxides post treatment. A region was chosen at a specific magnification with the backscattered electrons detector and were transferred into the EDX software for further analysis. In the chosen region, smaller regions, *regional spectrums*, were chosen independently, where the chemical composition were decided.

The same procedure was made for each coupon on all investigated sides.

3.1.6 SFE

The contact angle tests were conducted using the Attension® Theta Lite optical tensiometer [60] and the accompanying software OneAttension[61]. The metal coupon was placed and leveled in the tensiometer. A drop of liquid was dropped from a syringe onto the surface of the sample. Two different liquids were used to fulfil the requirements for using the OWRK method, and those were Milli-Q purified water and dimethyl sulfoxide. These liquids have known dispersive and polar contributions to the surface tension and the ratio between their contributions are variant. The values of these parameters is furthermore demonstrated in the Results section, Chapter 4.

Prior to the contact angle measurements, the liquids themselves were analyzed using the same experimental setup. The surface tension of the liquids were measured and compared to literature values. A margin of $\pm 1,0 mN/m$ was accepted to move on with the contact angle measurements. The measurements were divided into several sections, where both liquids were tested prior to every analysis section.

Three tests were performed for each sample, on the left, middle and right zones of the coupon. Each test consisted of an analysis of one droplet on the surface, measuring the left and right contact angle for all droplets. Two different samples of

the same metal/surface system were investigated and all values have been taken into consideration except for some outliers, making the final contact angle to be a mean value of 12 different angles for all coupons except for the Nickel based alloys, i.e. Alloy 6 and 7. These alloys surface morphologies differ from the other investigated alloys, since one side is brushed with equally large crevices perpendicular to the coupon sides. This kind of surface morphology is causing oval shaped droplets on the brushed side of the coupon upon investigation. Since the crevices are perpendicular to the sides of the coupons, three measurements were made for the brushed side, and then the coupon were turned 90°, and three more measurements were made. Futhermore, the other side, mill oxide, of the coupon was investigated with three more droplets. Accordingly, a total of 18 measurements were conducted for each Nickel coupon, and a mean value of these 18 was calculated to obtain the final value for the contact angle.

When all contact angles had been measured and collected, the mean value and standard deviation was calculated for all investigated coupons. Furthermore, a Python script was made in accordance with the OWRK method (2.3.2) and the literature values for DMSO and MilliQ water were added to the code. The measured contact angles for water and DMSO were added to the code individually for all coupons and the script output is the results used and demonstrated.

3.2 Fouling Test

A real time fouling analysis has been done at Kristineberg Marine Center, located on the Swedish west coast by the Gullmar fjord 80 kilometers north of Swedens second city Gothenburg. The Gullmar fjord is known for its variety of marine life and growth thereafter. One notable feature of the marine growth in the Gullmar fjord is the presence of large, dense forests of the kelp species Laminaria hyperborea. These kelp forests provide a vital habitat for a variety of marine organisms. [62] Since this project has a limited time frame, harsh corrosion and fouling environment is highly demanded to obtain relevant results in 11 weeks. Fortunately, the time period of the project also fits well with the time for blooming of certain marine organisms. Hence, microbial activity for these organisms is drastically increased during the project time compared to other timeslots around the year. The fouling test setup module is furthermore located approximately one meter below the surface and five meters from the shore to make the environment as harsh as possible regarding both corrosion and fouling aspects.

The fouling analysis can furthermore be divided into three major parts, where all of them are going to be contributing to the final result.

- Initiation and submerging of the metal coupons February 10th.
- Two visual checks during the eleven weeks of submerging. One check March 2nd, and the second check Mars 30th.
- Final check, April 26th. Coupons air dries and fouling is measured when the coupons are completely dry.

3.2.1 Initiation of Fouling Test

The fouling test was initiated on the 10th of February 2023 at Krisitneberg Marine Center. The test is containing 33 coupons, divided into seven different alloys and four different surface treatments. There are a total of 19 different material systems that are being investigated. All coupons that are in some way surface treated and the Copper based alloys are being investigated in a quantity of two because of any possible mistake during the treatment process. The bare stainless steels are only investigated in a quantity of one, since the margin of errors in manufacturing of these coupons is assumed to be negligible.

To submerge all of the coupons and to make sure all of them are staying in place during the testing time, a frame made out of galvanized steel was provided from Kristineberg Marine Center. The galvanization of the frame is necessary to prevent it from corroding, since the test is located in a very corrosive environment over time.

The coupons were furthermore adhered to the frame without any additional metallic materials to prevent the frame from acting as a cathodic protection to the coupons. Plastic cable ties and self adhesive rubber stripping were used to be the last component in the fouling setup, and were utilized as illustrated in Figure 3.2.

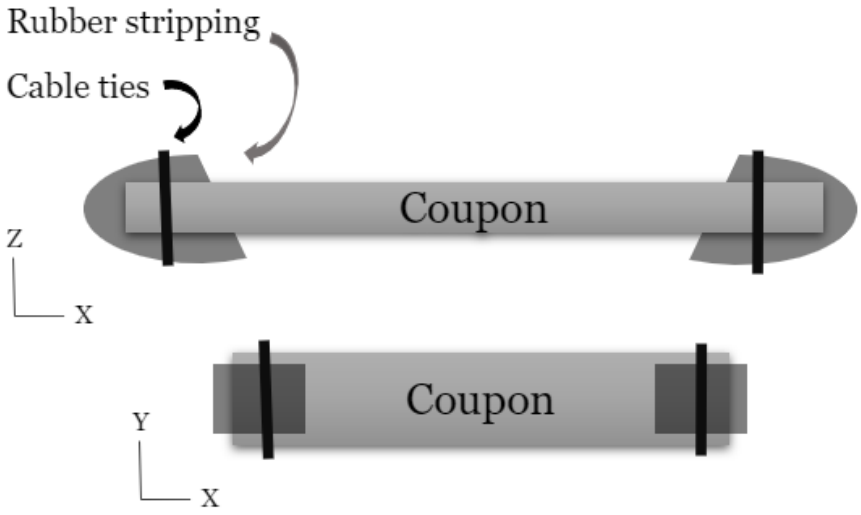

Figure 3.2: A visual representation of the fouling test coupon set up.

Some of the coupons are having different geometries, and thus tougher to attach to the frame. These coupons were therefore attached with an additional stripe in the x-direction between the two stripes which were attached in the y-direction on top of the rubber stripping to prevent the coupons from fall of the frame.

When all of the coupons were prepared, they were attached to the frame with two additional stripes, one on each side of the coupon. The positioning of the coupons was randomized to eliminate any risk of manipulating the results. All of the positions on the frame were given a number between 1 and 33, and thereafter randomizing which coupon to put at each position. When all of the coupons were attached to the frame, a final inspection of the attachments was made. When the setup was considered good, the *fouling module* was ready to be submerged. The final fouling module is furthermore displayed in Figure 3.3

Figure 3.3: The fouling test setup module prior to submerging. The dimensions is approximately 2 x 1 meters.

The last step in the fouling test initiation was the actual submerging. The module was attached to the dock at Kristineberg Marine Center with ropes tied to the metallic loops in the top corners in Figure 3.3 and through metallic loops drilled into the dock. The module were submerged approximately one meter below the surface, causing the coupons to be exposed to seawater in the depth of 1 to 2.5 meters.

3.2.2 Meantime Visual Inspections

During the test time, a few visual inspections of the fouling module were done to make sure that all of the coupons still were attached to the module, but also to visually inspect the fouling on the different coupons.

3.2.2.1 Emergency Inspection

About five days past the date of immersion of the module, the storm named "Otto" hit the Swedish west coast, specifically including the location of Kristineberg Marine Center. The storm caused quite large waves at the otherwise generally calm water conditions at the location.

The module was furthermore taken out of the ocean to inspect any failures on the module caused by the weather conditions, and not to inspect the marine growth on the submerged coupons. Once the module were taken out of the ocean, two of the coupons had been detached from the module on one side of the coupon. These coupons were furthermore attached to the module once again, but with an extra stripe to ensure further attachment throughout the fouling test upon bad weather conditions. All remaining coupons were however strongly attached to the module and did not require any additional measures.

3.2.2.2 First Inspection

The first inspection took place the 2nd of Mars 2023 at the test facility. The fouling module was taken out of the water completely to be able to analyze the growth onto the coupons. The coupons were photographed, still attached to the module. Once the visual analysis was done and the coupons had been photographed, the entire fouling module was submerged back into the ocean once again.

3.2.2.3 Second Inspection

The second fouling inspection occurred on the 31st of Mars 2023. The module was investigated similarly as during the first inspection, and photographs of the coupons were taken.

3.2.2.4 Final Inspection

The final inspection took place the 26th of April 2023, which is resulting in a total of 77 days of submersion. The entire module was removed from the dock and was taken into a boathouse for the final examinations. The module was furthermore

suspended to the roof in the boathouse with ropes to more easily investigate the module.

To measure the growth on each individual coupon, the additional fouling grown on the edges, attached to the ropes, plastic stripes and the metallic module itself was removed and the module was left with only the fouling attached to the coupons themselves. Once the additional fouling was removed, all of the fouling on a certain surface area on each coupon was collected and put onto a filter paper for drying. All of the filter papers were weighed before adding the fouling onto it, m_0, to make sure the weighing of the growth were accurate. The fouling were set to dry, for approximately two hours and twenty minutes, on the filter paper prior to the final weight. Lastly, all of the coupons were removed from the module and were cleaned with hot tap water to visually examine any MIC damage.

The filter papers were furthermore weighted on a scale with accuracy up to $0,01g$, and m_0 was subtracted from the final value displayed on the scale, m, to obtain the mass of the fouling attached to the coupon, m_f, in a certain area, A_f. The fouling value is expressed using the following equation:

$$\xi = \frac{m_f}{A_f}, \qquad \xi = \left[\frac{g}{cm^2}\right]$$

Since all of the coupons were submerged in copies of two, except for the bare stainless steel samples, the final value of the mass per area unit of each material system is a mean value between the fouling value of the two counterparts.

4

Results and Discussions

Presented in this chapter is, for each topic, first the results and data generated followed by discussion regarding the topic. The topics are as follows: morphological and compositional data generated using SEM and EDX. The materials' calculated SFE, along with the polar and dispersive contribution, and their average contact angle. The results from the fouling test taking in account both marine fouling and corrosion. The data shown is also explained and discussed based on the theory introduced in Chapter 2. Lastly, presented at the end of this chapter is discussion regarding the economical, environmental and ethical aspects for the energy sector in general, but also for this particular project, its extent and the materials being used.

4.1 SEM Results

Analyzing Alloy 1 - Bare compared to when treated, Coating 1, (a) and (c) compared to (b) and (d) in Figure 4.1, there is not much difference. The divergence in shade is due to the change in voltage, for instance 20kV in (a) and 10 kV in (b). When considering the images (c) and (d) in Figure 4.1, it is evident that particles have aggregated on the surface after treatment. The aggregates appear as bright spheres on the surface of the sample.

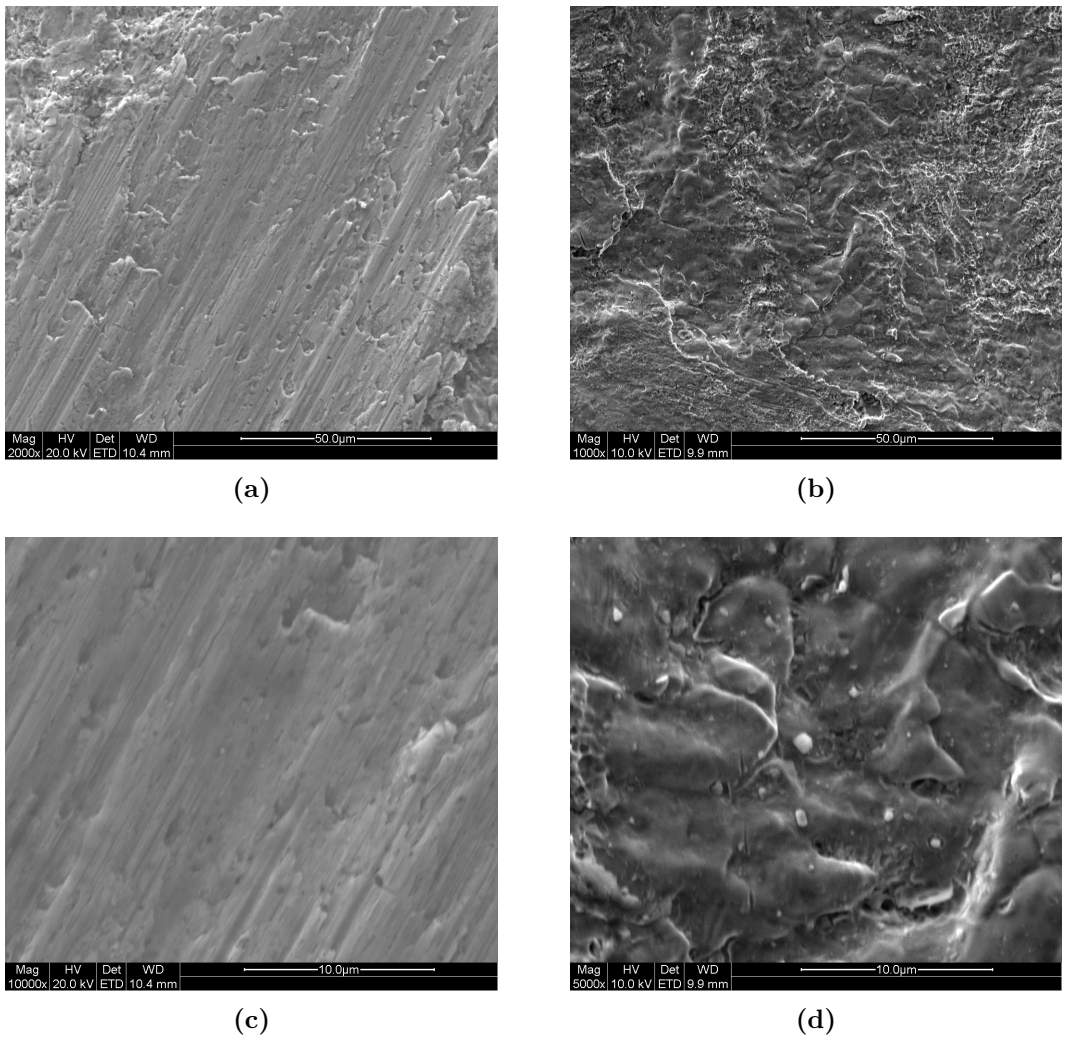

(a) **(b)**

(c) **(d)**

Figure 4.1: SEM analysis with a length for scale of 50 μm for (a) Alloy 1 - Bare and (b) Alloy 1 - Coating 1, and analysis with length scale of 10 μm for (c) Alloy 1 - Bare and (d) Alloy 1 - Coating 1.

Similar to Alloy 1, one can observe aggregates formed on the surface of Alloy 2 - Coating 1, Figure 4.2, (b) and (d), not previously found for Alloy 2 - Bare, Figure 4.2 (a) and (c).

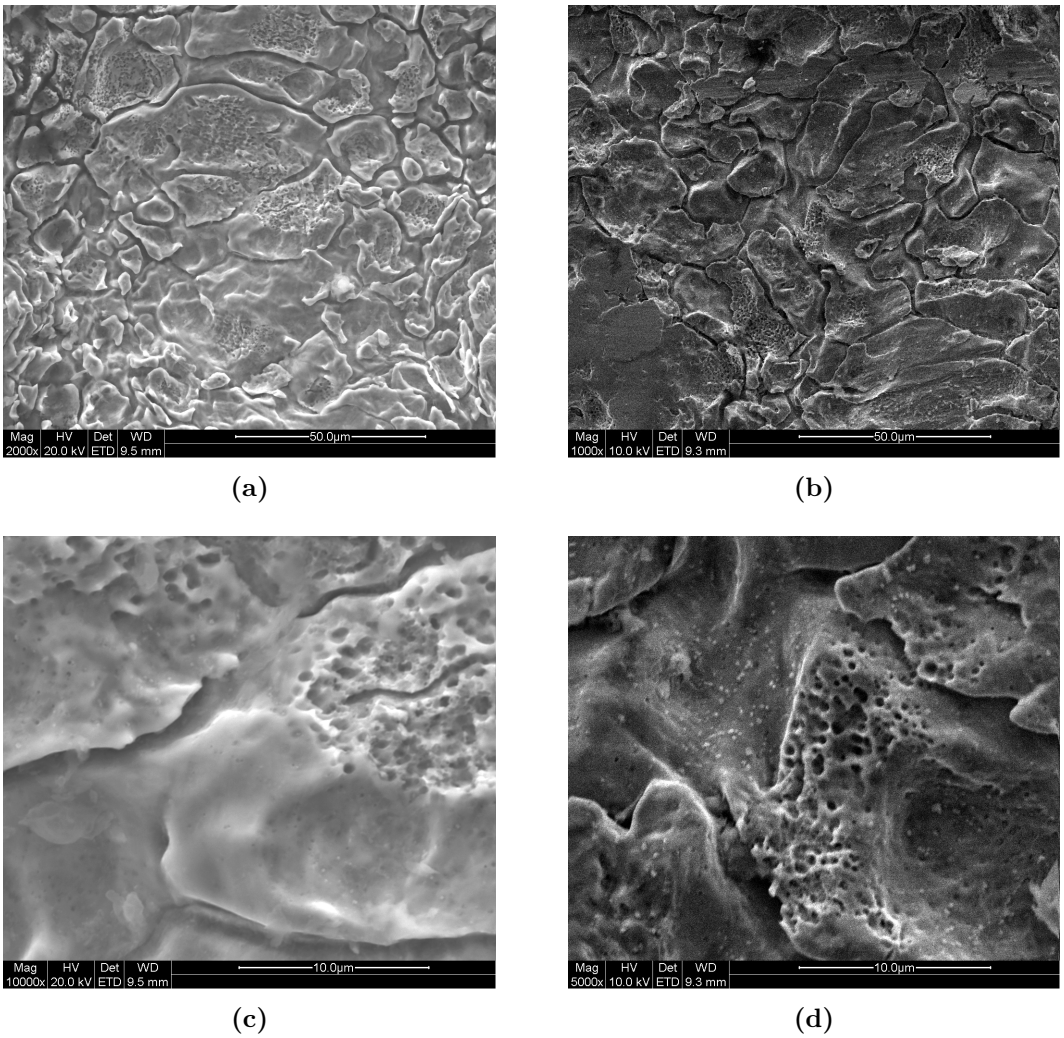

(a) **(b)**

(c) **(d)**

Figure 4.2: SEM analysis with a length for scale of 50 μm for (a) Alloy 2 - Bare and (b) Alloy 2 - Coating 1, and analysis with length scale of 10 μm for (c) Alloy 2 - Bare and (d) Alloy 2 - Coating 1.

The results observed in Figure 4.3, where Alloy 3 - Bare, is compared to Alloy 3 - Coating 1, show deviation from the trends of Alloys 1 and 2 by not having formed as many aggregates. Another difference shown is Alloy 3 being considerably less porous than Alloy 1 and 2.

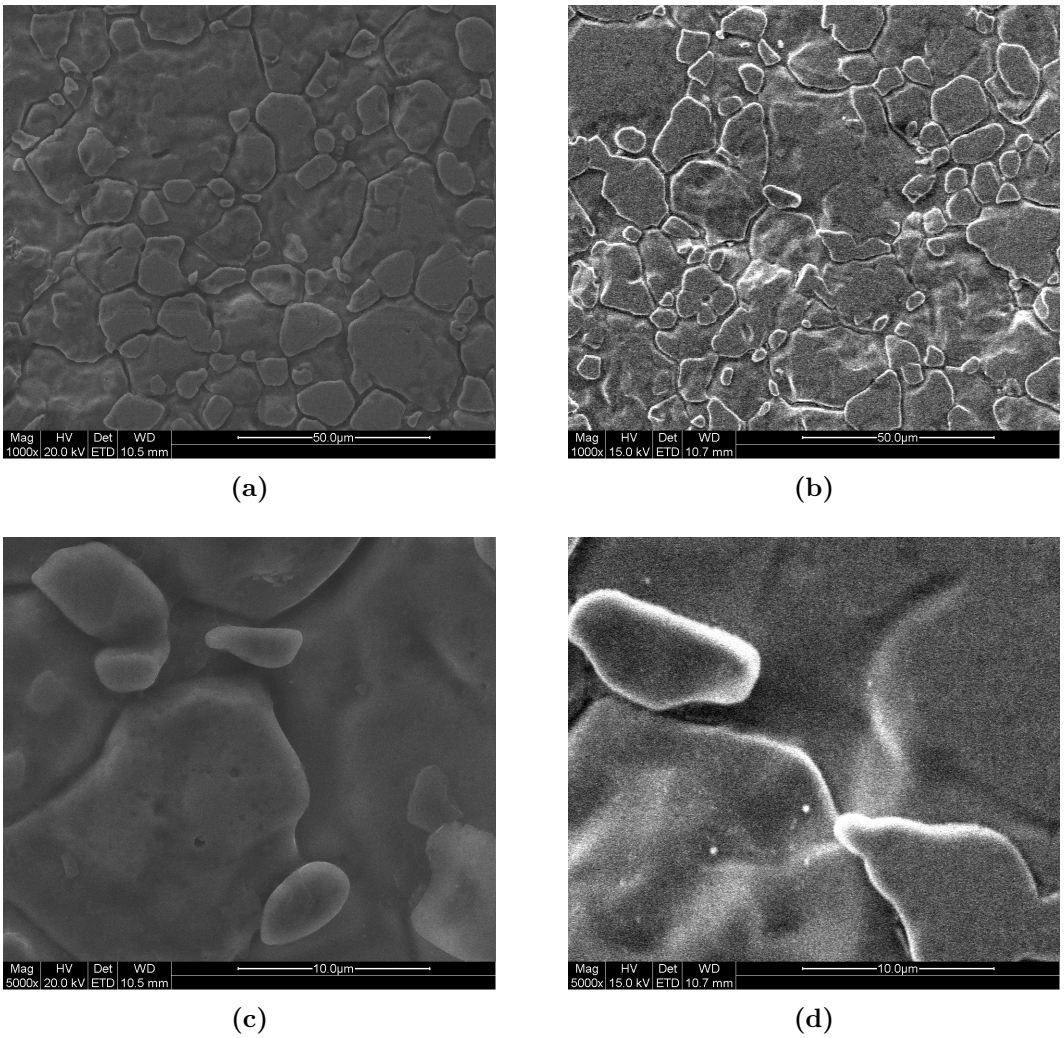

(a) **(b)**

(c) **(d)**

Figure 4.3: SEM analysis with a length for scale of 50 μm for (a) Alloy 3 - Bare and (b) Alloy 3 - Coating 1, and analysis with length scale of 10 μm for (c) Alloy 3 - Bare and (d) Alloy 3 - Coating 1.

When comparing the Alloys 1-3, bare and surface treated, Figure 4.1 - 4.3, the apparent difference is as mentioned the addition of particles on the surface. Hence, the difference in micro-structure of the surface, before and after surface treatment, is negligible. In all these figures, the characteristic grain boundaries and porosity is present, regardless.

Additionally, an image of Alloy 1 - Coating 2, Figure 4.4, was generated using SEM and capturing the topological data of the side of the sample (perpendicularly towards the XZ-plane according to Figure 3.2. As opposed to the XY-plane which is the case when otherwise not mentioned). The surface roughness is evidently greater for the side of the sample while only a few aggregates are visible on the surface.

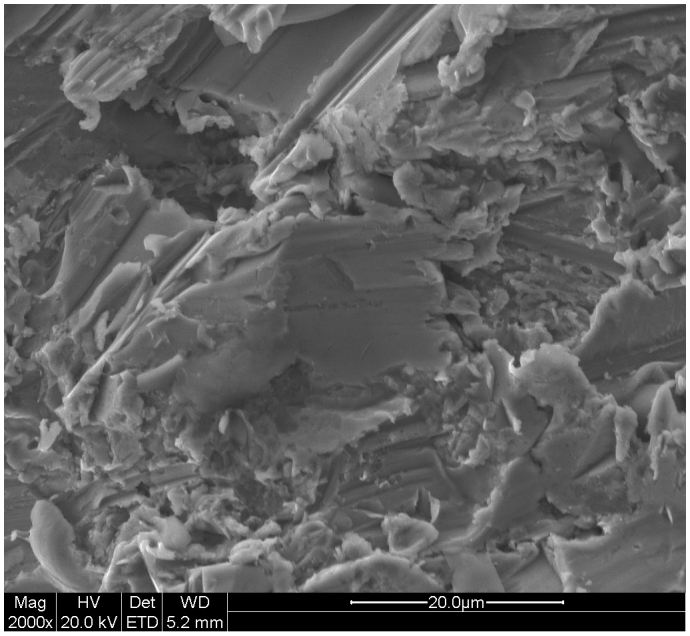

Figure 4.4: SEM analysis with magnitude x2000 of Alloy 1 - Coating 2. Image taken of the edge of the sample.

Furthermore, only a qualitative, visual analysis of the topology of the samples has been made so far. The surface treatment seems to have only affected the composition of the surface while not affecting the actual structural component of the treated surface.

4.1.1 EDX Results

For all Tables in this section, the weight percentages of the elements of interest, Oxygen, Chromium and Yttrium are presented. The values were calculated by dividing the weight percentage of the specific element for each spectrum with the sum of the weight percentages of the above mentioned elements of interest. The data collected using the EDX apparatus however also included other elements, to be found in Appendix D.

4.1.1.1 Stainless Steel Alloys

To examine the samples and aggregates further, the composition was analysed using EDX. In Figure 4.1, the image from the SEM analysis is highlighted indicating the location of the surface the compositional analysis, Table 4.1, were conducted.

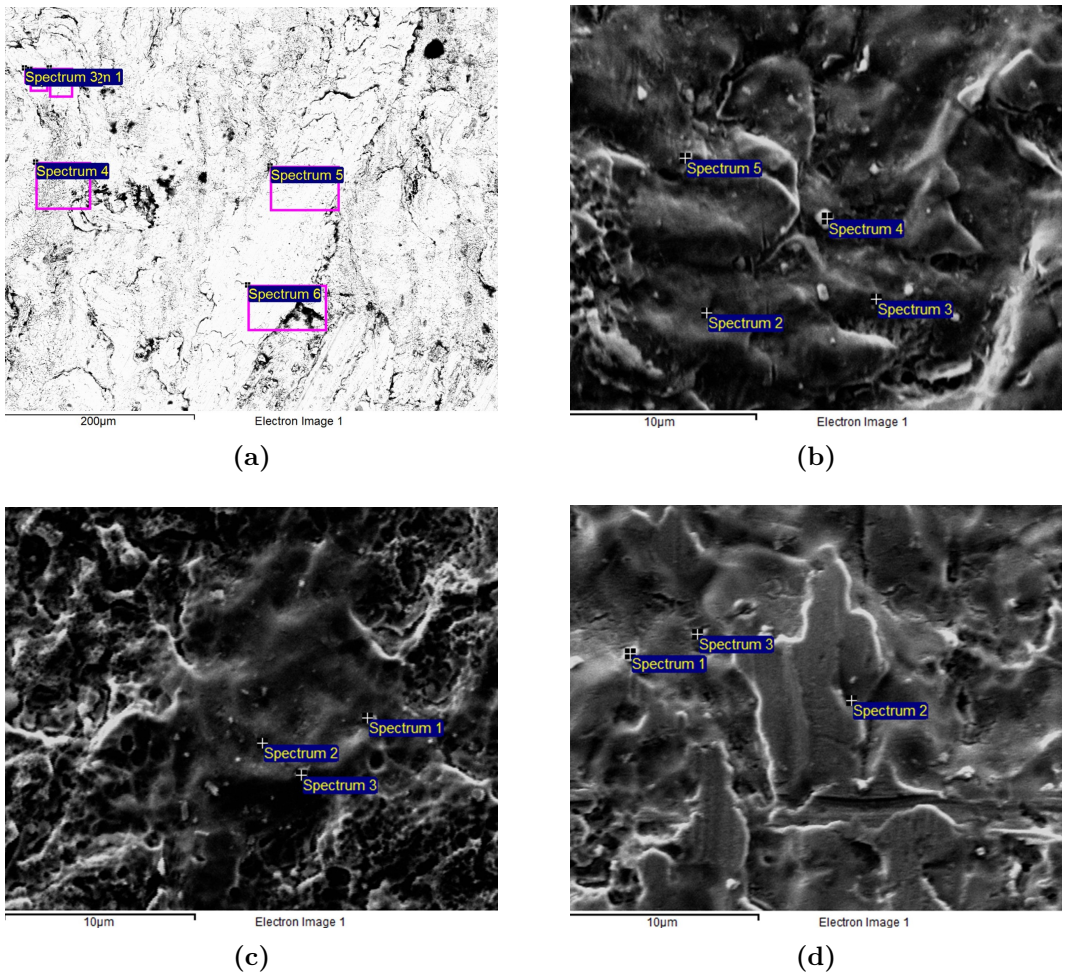

Figure 4.5: Image used and specified spectra in the EDX analysis for (a) Alloy 1 - Bare, (b) Alloy 1 - Coating 1, (c) Alloy 1 - Coating 2, (d) Alloy 1 - Coating 3

No peak was found indicating the presence of Yttrium, therefore the EDX analysis, Table 4.1, does not include it for Alloy 1 - Bare. In Figure 4.5 (b), spectra 4 and 5 are located upon two different aggregates while spectra 2 and 3 are located generally on the surface. When comparing this to the values in Table 4.1 the conclusion can be drawn that the aggregates experience a higher concentration of Yttrium. In spectrum 4, the amount of Oxygen is considerably greater than for surrounding spectra. Observing Coating 2 and 3, the trend of increased Oxygen levels with the presence of Yttrium levels is apparent.

Table 4.1: Weight percentages of the elements of interest in Alloy 1: Bare, Coating 1, 2, and 3. Analysed using EDX.

Spectrum	**O**	**Cr**	**Y**
Alloy 1 - Bare			
1	11,43	88,57	-
2	9,64	90,36	-
3	8,00	92,00	-
4	2,93	97,07	-
5	4,26	95,74	-
6	4,68	95,32	-
Alloy 1 - Coating 1			
2	6,98	91,20	1,82
3	9,51	87,74	2,75
4	58,32	35,87	5,81
5	12,64	82,23	5,13
Alloy 1 - Coating 2			
1	31,03	61,85	7,12
2	8,10	90,94	0,96
3	58,18	36,96	4,86
Alloy 1 - Coating 3			
1	75,49	17,13	7,38
2	15,29	70,98	13,73
3	36,83	41,47	21,70

The analysis of Alloy 2 includes only the bare sample and Coating 1. In Figure 4.6 the spectra chosen are indicated in each image. Observing Figure 4.6 (b), one will notice that there more aggregates on the surface but the size of the aggregates are however smaller than compared to the previous images of Alloy 1 , Figure 4.5 (b) - (d).

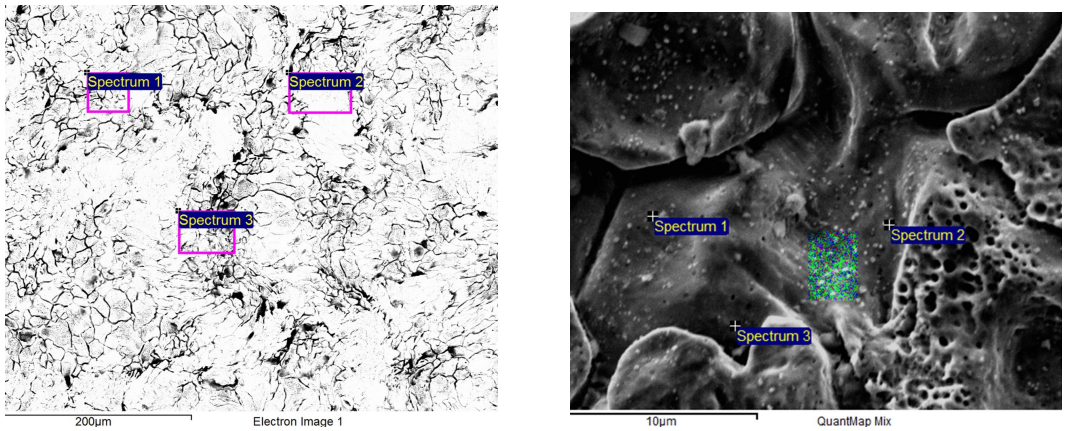

(a) **(b)**

Figure 4.6: Image used and specified spectra in the EDX analysis for (a) Alloy 2 - Bare (b) Alloy 2 - Coating 1

The increase of Oxygen is largest when the increase of Yttrium is lowest. Furthermore, the amount of Oxygen is similar to that of the bare sample and the Chromium concentration has however decreased. Specifically, Chromium decreases as Yttrium increases.

Table 4.2: Weight percentages of the elements of interest in Alloy 2 - Bare and Coating 1.

Spectrum Alloy 2 - Bare	**O**	**Cr**	**Y**
1	14,57	85,43	-
2	9,11	90,99	-
3	17,41	83,13	-
Alloy 2 - Coating 1			
1	16,98	80,09	2,93
2	12,93	76,65	10,42
3	14,63	69	16,38

In Figure 4.7 three spectra are indicated in each image and analysed using EDX. In image (b), the aggregates are reasonably visible on the flat surface of Alloy 3. Compared to the image of Alloy 2 - Coating 1, Figure 4.6 (b), the aggregates on the surface are smaller for Alloy 3 - Coating 1 (additionally, notice the difference in scale of the two images, Figure 4.6 and 4.7).

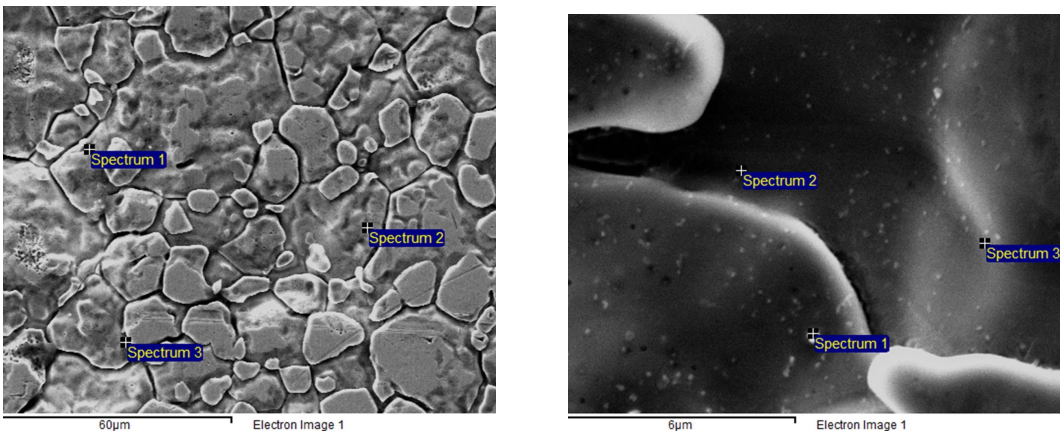

(a) **(b)**

Figure 4.7: Image used and specified spectra in the EDX analysis for (a) Alloy 3 - Bare (b) Alloy 3 - Coating 1

Following the visual inspection above, the EDX analysis, Table 4.3, show that the aggregate analysed in spectrum 1 have generally high concentrations of Oxygen and Yttrium. Spectrum 2 shows an increase in both Yttrium and Oxygen concentration while spectrum 3 have similar concentrations of oxygen as Alloy 3 - Bare.

Table 4.3: Weight percentages of the elements of interest in Alloy 3 - Bare and Coating 1, generated using EDX.

Spectrum Alloy 3 - Bare	**O**	**Cr**	**Y**
1	3,39	96,61	-
2	2,95	97,05	-
3	0,15	99,85	-
Alloy 3 - Coating 1			
1	25,62	63,73	10,65
2	7,57	85,47	6,96
3	2,75	94,61	2,64

Lastly, the spectra highlighed in the image of Alloy 1 - Coating 2, Figure 4.8, were analysed using EDX generating data from the side of the sample, as mentioned above: perpendicular to the XY-plane. Figure 4.8 looks a bit different to the SEM-image, Figure 4.4, which is because of the difference voltage used during the analyses. It is also different in regards to the other images of the EDX-analyses post surface treatment, since no aggregates are visible in Figure 4.8.

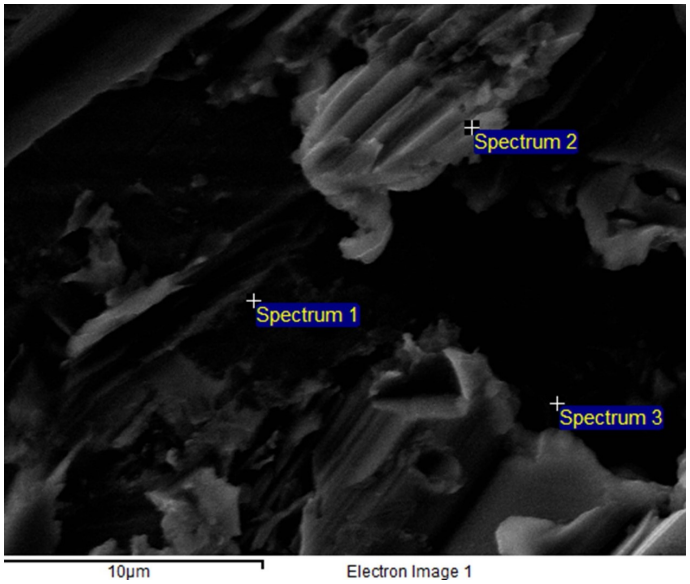

Figure 4.8: Image used and specified spectra in the EDX analysis for Alloy 1 - Coating 2. Image taken of the edge of the sample.

Although no aggregates are visible in Figure 4.8, Yttrium can still be proven to be present within the surface, see Table 4.4. Compared to the bare sample of Alloy 1, both Oxygen and Yttrium has increased. Spectrum 3 especially, but also Spectrum 2, indicate high concentrations of Yttrium.

Table 4.4: Weight percentages of the elements of interest in Alloy 1 - Coating 2, edge of sample. Generated using EDX.

Spectrum Alloy 1 - Coating 2	**O**	**Cr**	**Y**
1	54,53	42,22	3,25
2	32,48	58,82	8,7
3	56,73	24,67	18,6

The size of the aggregates are different depending on the alloy. By visually inspecting the images presented above approximate sizes of the aggregates are deduced. For Alloy 1, the smallest aggregates are approximately 200nm while the largest is almost 1000nm (Figure 4.5 (b) - Spectrum 4), however most larger aggregates are around 600nm. Alloy 2 has the most uniform spread in size distribution of the aggregates, the smallest visible from 100nm, to the biggest of around 400nm. However, Alloy 3 has many uniformly shaped aggregates of around 100nm in diameter with a few larger ranging up to 300nm.

4.1.1.2 Nickel Alloys

Although not presented in the SEM section, Alloy 6 and 7 were analysed in using SEM then EDX. In Figure 4.9 both the alloys' topology and their spectra can be observed. The SEM/EDX were conducted on the mill oxide side of the nickel coupons and as seen in the images, both coupons have some degree of surface roughness such as pores and groves.

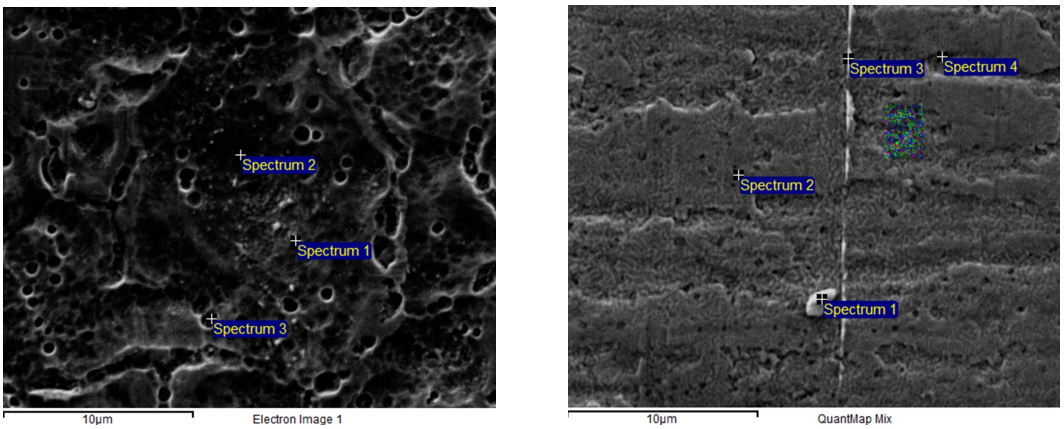

(a) **(b)**

Figure 4.9: SEM-generatred image used and specified spectra in the EDX analysis for (a) Alloy 7 - Coating 1 (b) Alloy 6 - Coating 1.

Primarily, evaluating Table 4.5, Alloy 7 - Coating 1, spectrum 3 stands out with the highest concentration of Yttrium yet: 45,99 weight percent. However, both nickel alloys (Alloy 6 and 7) present generally high concentrations of Yttrium. The Oxygen concentration of Alloy 7 spectrum 1 is similar to that of spectrum 3, but

the Yttrium concentration is not nearly as high as in spectrum 3. Spectrum 1 is analyzing a general part of the image while spectrum 3 is located in one of the groves or pores, 4.9 (a). Spectrum 2 has the highest concentration of Chromium for Alloy 7, although similar values of Chromium to spectrum 1. Except for spectrum 3 for Alloy 7, Chromium has the highest percentage in both Alloy 7 and 6. In Alloy 6, the Oxygen concentration is similar to that of Alloy 1 - Coating 1. For Alloy 6, spectrum 1 analyses an aggregate on the surface while spectrum 3 is set on a bright area stretching all across the image, Figure 4.9, (b). In spectrum 1 and 4 for Alloy 6, the Oxygen concentration is generally higher and the Chromium concentration lower.

Table 4.5: Weight percentages of the elements of interest in Alloy 6 and 7 - Coating 1, generated using EDX.

Spectrum Alloy 7 - Coating 1	O	Cr	Y
1	24,67	63,33	12,00
2	12,00	67,79	20,20
3	22,36	31,65	45,99
Alloy 6 - Coating 1			
1	43,92	49,64	6,44
2	9,53	75,85	14,62
3	10,13	78,37	11,51
4	31,87	55,53	12,6

4.2 SEM and EDX Discussion

As mentioned above in Section 4.1, stainless steel Alloy 3 exhibits a less rough surface than Alloy 1 and 2, which also are stainless steels. The surface roughness could be a reason why Alloy 3 is less affected by the surface treatment. When only considering the SEM analysis, a difference in Yttrium concentration cannot be quantitatively determined. However, the EDX data clearly present higher concentration of Yttrium for Alloy 2 and somewhat for alloy 1, supporting the claim that surface roughness to some degree affects the Yttrium nanomaterial surface treatment. When comparing the images of a bare and of a surface treated sample, it is apparent that the structure of the surface is unaffected by the treatment.

The surface roughness is clearly significantly higher at the edge of the sample, Figure 4.4, and the concentration of Yttrium are higher compared to that of the other areas on the corresponding sample. Compared to the stainless steels, Alloys 1-3, the nickel based Alloys 6 and 7, contain generally high concentrations of Yttrium. Spectrum 3, for Alloy 7 treated in *low temperature - short time*, in particular have extremely high amounts of Yttrium and is located within a pore or grove of the surface. This could imply that the nanoparticles from the solution gather in pores and crevices during dipping of the coupon. Although, if this is favourable and something to strive for is still undefined. The morphology of Alloy 6 however does not seem to allow for such extreme accumulations of Yttrium. Although, spectrum

2 and spectrum 4 show an increased amount of Yttrium, probably due the the same phenomenon. However, it is not stated or proven that the highest concentrations of Yttrium will generate superior properties of the nanomaterial surface treatment. Nor is it the aggregates on the surface that is the most important result from the treatment. When analyzing the spectra located on the general surface in the image and not on the aggregate, there is still Yttrium and Oxygen present, but small enough to not appear in the SEM image. From this, it is reasonable to claim that a nanooxide layer has formed on the surface. This is not to confuse with adding a coating layer to the surface since there is no interface between the protective nano-oxide and the alloy, it is rather an addition of nanoparticles to the surface, thermally growing a protective oxide layer. This thin protective oxide layer formed can then technically be compared to the TGO used in TBCs, with similar properties. As stated in the Theory: Yttrium and Aluminum have similar behaviour and Aluminum is the most used TGO material, following that the surface treatment investigated in this study should make the surface of the alloy non-permeable to oxygen due to its small grain size.

Regarding the composition of Yttrium, Chromium and Oxygen present on the surface caught with the EDX detector in the microscope, there is a slight deviation between the different spectra. In the SEM pictures, light coloured clusters were believed to be clusters of oxides containing both Chromium and Yttrium which the EDX analysis furthermore confirmed. These clusters are aggregates of Yttrium, Chromium and Oxygen and is an indication of the composition of the protective oxide itself. Since the EDX detector is scanning radiation from X-Rays generated by electrons which has been penetrating the surface a few micrometers, some peaks is going to be caught from the bulk of the material. While investigating the aggregates, a higher percentage of investigated material will be the aggregate, illustrated in Figure 4.10, causing the composition values at these clusters more accurately represent the composition of the protective oxide. This conclusion can be drawn since the clusters of nanoparticles in the solution are oxidizing in the same way as the single nanoparticles on a metallic surface upon air vented heat treatment.

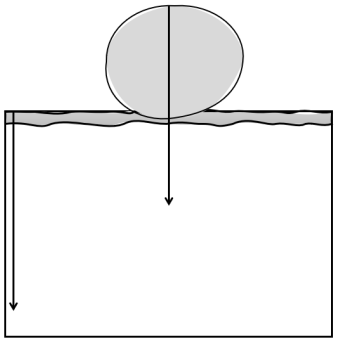

Figure 4.10: An image illustrating the approximate depth of the EDX analysis. Where the aggregate sits on the surface with the TGO layer grown within the alloy. Emphasizing that this image is merely a visualization of the EDX principle and not a representation of the shape of the actual aggregate.

In certain alloys, the oxide clusters are demonstrated as light dots in a darker image, and for other alloys it is not as easy to visualize. For the alloys without obvious oxide clusters, the spectrum containing the highest amount of oxides was considered the most correct spectrum. In all spectra containing the highest amount of Oxygen, there are obvious amounts of both Chromium and Yttrium present, where the weight percentage of Chromium is higher than for Yttrium in all cases. This is due to the higher amount of Chromium in the alloy than the small amount of Yttrium adhered on the surface as a result of the coating and heat treatment procedures. This support the claim that the protective oxide layer has a thickness which is considerably less than the depth of the electrons that penetrate the sample. Also, it can be concluded that there are both Chromium and Yttrium rich oxides present on the surface for all alloys investigated after treatment. The newly altered chemical composition on the surface is furthermore a combination of two different protective oxides, Cr_2O_3 and Y_2O_3, where the second has some interesting properties. Rare earth elements are known to apply the *Reactive Element Effect*, causing the metallic surface to be more oxygen reactive than scale forming, hence hindering corrosion.

4.3 SFE Results

In Table 4.6 below, the contact angles between the specimen and the liquid is displayed. The contact angles below is a mean value of 12 contact angles on the same specimen.

Table 4.6: Contact angle measurements for MilliQ-water on the test specimens documented below

Material System	Contact Angle	Standard deviation
Alloy 1 - Coating 1	109,79°	0,84°
Alloy 1 - Coating 2	107,19°	1,51°
Alloy 1 - Coating 3	104,22°	1,48°
Alloy 1 - Coating 4	88,01°	1,23°
Alloy 1 - Bare	48,32°	3,15°
Alloy 2 - Coating 1	103,40°	1,25°
Alloy 2 - Coating 2	102,26°	0,69°
Alloy 2 - Coating 3	108,82°	1,08°
Alloy 2 - Coating 4	90,21°	0,71°
Alloy 2 - Bare	44,67°	3,18°
Alloy 3 - Coating 1	97,41°	3,45°
Alloy 3 - Coating 2	104,24°	1,59°
Alloy 3 - Coating 3	105,86°	2,11°
Alloy 3 - Bare	69,39°	1,35°
Alloy 4 - Coating 4	86,16°	2,20°
Alloy 4 - Bare	58,57°	3,73°
Alloy 5 - Bare	84,08	2,80
Alloy 6 - Coating 1	107,17°	19,25°
Alloy 7 - Coating 1	104,86°	19,48°

Interestingly, the contact angle increased by extreme measures for Coating 1, 2 and 3, but also Coating 4 compared to the bare metal. This trend is true for both Alloy 1 and 2, which puts emphasis on the permanence and reliability of the data. The most extreme contact angles measured using MilliQ-water is for Alloy 1 - Coating 1 and Alloy 2 - Coating 3. However, no conclusion regarding preference between Coating 1,2, or 3 can yet be made. The standard deviation for these measurements are also reassuring being less than 3,18°, not considering the bare alloys which have a standard deviation of 1,51° at most. It is clear from these results that Coatings 1,2, and 3 increase the contact angle significantly, regardless of the alloy used. This is also true for Coating 4, yet not as large of an increase in contact angle.

Some concerning values of standard deviation can be seen in the bottom of Table 4.6. Anyway, the high value is due to the morphology of the samples. The measurements generating these results are due to one side of the sample being brushed, causing the drop to spread only in one direction. Therefore, these results shall be divided and reevaluated.

Table 4.7: Contact angle measurements for DMSO on the test specimens documented below

Material System	**Contact Angle**	**Standard deviation**
Alloy 1 - Coating 1	60,85°	2,39°
Alloy 1 - Coating 2	56,92°	2,83°
Alloy 1 - Coating 3	55,97°	1,84°
Alloy 1 - Coating 4	58,05°	0,89°
Alloy 1 - Bare	30,75°	1,33°
Alloy 2 - Coating 1	62,49°	5,63°
Alloy 2 - Coating 2	46,92°	2,45°
Alloy 2 - Coating 3	48,46°	1,11°
Alloy 2 - Coating 4	59,81°	2,65°
Alloy 2 - Bare	35,11°	1,68°
Alloy 3 - Coating 1	60,13°	1,67°
Alloy 3 - Coating 2	57,43°	2,19°
Alloy 3 - Coating 3	57,05°	2,04°
Alloy 3 - Bare	43,94°	3,31°
Alloy 4 - Coating 4	49,47°	3,20°
Alloy 4 - Bare	14,36°	2,28°
Alloy 5 - Bare	50,97°	3,70°
Alloy 6 - Coating 1	57,14°	14,92°
Alloy 7 - Coating 1	54,55°	10,18°

Similar trends of increased angles can be found in the DSMO measurments, although the measured angles are not as extreme. Deviating from the trend is however the large increase in contact angle, for Alloys 2 and 3, is Coating 1.

The contact angles presented in 4.6 and 4.7 are furthermore processed to display the different SFEs corresponding to each surface investigated. The values have been processed using Python[63], all calculations are presented in Appendix C, with reference to equations 2.6 and 2.7, as well as the constants presented in Table 4.8.

Table 4.8: SFE values with polar and dispersive contributions of the liquid used.

Liquid	**Total Surface Tension** $[mN/m]$	**Dispersive** $[mN/m]$	**Polar** $[mN/m]$
H_2O	72.8	22.8	50.0
DMSO	43.5	34.8	8.7

Table 4.9: SFE measurements of tested specimens with polar and dispersive contributions.

Material System	**Total SFE** $[mN/m]$	**Dispersive** $[mN/m]$	**Polar** $[mN/m]$
Alloy 1 - Coating 1	32,77	32,58	0,19
Alloy 1 - Coating 2	34,53	34,42	0,11
Alloy 1 - Coating 3	33,06	33,06	0,00
Alloy 1 - Coating 4	25,43	20,17	5,26
Alloy 1 - Bare	50,47	35,41	15,06
Alloy 2 - Coating 1	26,77	26,54	0,23
Alloy 2 - Coating 2	39,83	39,79	0,04
Alloy 2 - Coating 3	44,86	44,06	0,80
Alloy 2 - Coating 4	24,58	20,20	4,38
Alloy 2 - Bare	53,84	41,80	12,04
Alloy 3 - Coating 1	25,84	24,54	1,30
Alloy 3 - Coating 2	31,74	31,73	0,01
Alloy 3 - Coating 3	33,32	33,30	0,02
Alloy 3 - Bare	35,01	18,67	16,34
Alloy 4 - Coating 4	29,75	25,38	4,37
Alloy 4 - Bare	45,04	25,47	19,57
Alloy 5 - Bare	28,88	22,89	5,99
Alloy 6 - Coating 1	34,30	34,20	0,10
Alloy 7 - Coating 1	34,90	34,88	0,02

As shown in Table 4.9 the data is consistent with the theory where the SFE is lowered accompanying increased contact angle. When observing the data closer for the nanomaterial based surface treatments, i.e. Coating 1, 2 and 3, they are presented with another extreme phenomenon. The surface treatments have completely eliminated the polar contribution to the SFE while not affecting the dispersive contribution nearly as much. This conclusion could be drawn regarding the standard deviation of the contact angles for each of the coupons treated with Coating 1, 2 and 3, where the standard deviation of the polar contribution to the SFE is larger than the polar contribution itself for each of the coupons. This is only apparent for the nanomaterial surface treatments, while the PTFE paint coating, Coating 4, still indicate both dispersive and polar contributions to the SFE, but with lower values than for the bare metals, resulting in a lower total SFE. On the other hand, for Alloy 1 - Coating 1,2, and 3, it is shown that the dispersive contribution to the SFE of the bare alloy does not change much once it has been surface treated, it stays almost the same. For Alloys 2 and 3, a slight fluctuation of the dispersive contribution is demonstrated.

Alloy 4 - Bare has a slightly lower SFE than the other steel alloys but can not be associated with having better antifouling properties following its high degree of destruction due to corrosion in the fouling test.

Alloy 5 - Bare is the only alloy which has similarly low SFE as any alloy together with Coating 1,2,3, and 4. Interestingly, it has most similar values as any alloy and Coating 4, also considering the ratio between dispersive and polar SFE. This is

not apparent when comparing the results from the fouling test where Alloy 5 shows superior antifouling properties. This was however expected following the theory and history of copper alloys commonly used in marine environments.

4.4 SFE Discussion

Regarding the results following the nanomaterial based surface treatment where the surface experiences a complete elimination of the polar contribution to the SFE, the explanation is found within the new value of the EWF. As being demonstrated in Table 2.1, Yttrium and its oxide, Yttria, experience a lower EWF value than the base materials in Alloy 1-3 and Alloy 6-7, i.e. Iron and Nickel. As being demonstrated in Section 4.1, the surface treated alloys experience content of both Chromia, Cr_2O_3 and Yttria, Y_2O_3 on its surfaces. And as in Table 2.2, the difference in EWF for these oxides is significant. This implies a higher EWF for surfaces containing the majority of Chromia and Chromium than for Yttria and Yttrium induced surfaces. Since all coupons treated with Coating 1-3 are experiencing generally higher concentration of Yttrium and oxides, it can be concluded that Yttria is present on the coupon surface and therefore the total EWF value of the metallic surfaces has been decreased. A low EWF on the metallic surface is decreasing the energy required to remove electrons from its shells, which means that for surfaces with a lot of charge variation, electron movement neutralize the charge distribution. Negatively charged particles are acting as electron donors and providing electrons to particles which are positively charged. Hence, the theoretical framework in combination with the given results speaks for the fact that an even charge distribution is able to decrease the permanent dipole moment and hence decreasing the polar contribution to the SFE.

In some cases, the dispersive contribution to the SFE is not affected at all by the surface treatment. This is an indication of small or no differences in electron density fluctuations compared to the bare alloy. This is the case for Alloy 1, which has the highest alloying grade of the investigated stainless steels. For the other stainless steels, the dispersive contribution varies upon finished surface treatment, while the polar contribution is completely eliminated. By investigating these results, a conclusion can not be drawn regarding the dispersive contribution to the SFE upon treatment. The dispersive part of the SFE could therefore be classified as *Alloy Dependent*, when performing surface treatments like these. This implies that different changes for the dispersive contribution is highly dependent on the alloy's composition. Regarding the differences in surface free energy for the different heat treatment parameters for the surface treatment, various results has been presented. For Alloys 1, 6 and 7, similar SFE results are being demonstrated for all treatments, while for Alloys 2 and 3 the results are deviating. For Alloy 2 - Coating 1, there is a slightly higher standard deviation for the DMSO contact angle, which indicates that some of the used values when calculating the contact angle for this alloy probably were a lot lower than the actual contact angle and hence the value for the SFE is lower than the other alloys. The dispersive part of the SFE is decreasing upon higher DMSO contact angle. The contact angles for DMSO on the different surface treated coupons are very similar except for Alloy 2, where the least deviating values are experiencing a lower contact angle. Hence, it can be concluded that the nan-

otreatment combined with Alloy 2 is experiencing a more dispersive surface than for the other nanoparticle treated alloys. As being mentioned earlier, the dispersive contribution is highly dependent on the alloys composition. Alloy 2 does have less Chromium present in the total composition compared to the other alloys containing Chromium in an interval from 19 to 23 wt% while Alloy 2 contains approximately 13 wt%. This is furthermore the cause for the increased dispersive forces in Alloy 2 and it does also confirm the hypothesis that there should be minimal deviation between the different treatment methods, but that the alloy itself does contribute to the final SFE result. Another deviant result is the SFE for Alloy 3 - Coating 1, which is the considerably low value for the SFE, but also the polar contribution present in this material system. The total SFE is approximately six mN/m lower than the other material systems containing similar amount of Chromium. For this coupon, the contact angle for water is significantly lower compared to the other coupons and with a higher standard deviation. A lower total contact angle for water implies a small polar contribution to the SFE according to Equation 2.8, which disputes the theory about rare earth elements in metallic alloys. However, Alloy 3 was cut into coupons using sheet metal scissors at the manufacturer, unlike for the other alloys which were cut by water jet. Additionally, Alloy 3 is made from a thinner sheet than the other stainless steels, which has caused the coupons to be slightly concave. While investigating these coupons in the tensiometer, the camera were not able to directly find the metallic surface since it was not completely flat. The contact angles were furthermore produced on a non flat surface, hence the angles are both deviating and slightly lower than for other coupons. Later in this section, some additional sources of error are going to be discussed, and the results with the deviating values are furthermore very likely to be caused by these sources besides the obvious causes mentioned above.

It seems that the alloy used for Coating 4 do not affect the SFE of the coating. Considering that Coating 4 is an actual coating, by definition, one material is put upon another and the base material will not affect the the coating in regards to SFE. Hence, it is expected that the measurements for all alloys with Coating 4 are similar.

The lowest surface energy obtained for a non treated coupon was found for the Copper based alloy, Alloy 5. The total surface energy for Alloy 5 is less than any coating treated with the nanotreatment, i.e. Coatings 1-3. This is mainly a result from the hydrophobicity Copper experiences, and not a result of the alloying grade itself unlike the case for stainless steels where an addition to the alloy is decreasing the SFE and hence increasing the hydrophobicity. The hydrophobicity is due to the oxide layer present on the Copper alloys, which also one of the biocidal part of the alloys surface. [64] Alloy 5 is investigated because it is known to be a great alternative in subsea applications, but industries want to get rid of copper in their equipment because of the environmental aspects even though its performance is impeccable. Except for the biocidal properties of Copper, it is a very expensive material causing the CAPEX value for a subsea cooler to drastically increase and the financial profit margins to decreases.

The Nickel alloys investigated, Alloy 6 and 7, have been treated with one of the same treatment as all of the stainless steel coupons, Coating 1, which is the

low temperature - short time treatment of the nanoparticle surface treatments. The results of the analysis for these particular alloys does get affected very similarly to the stainless steels treated with the same treatment method, causing the polar contribution to be completely eliminated. This conclusion can be drawn similarly as for the rest of the coupons, i.e. since the standard deviations for the contact angles are resulting in a larger deviation for the polar contribution than for the final value of the polarity itself. The standard deviation for the contact angles is a lot higher than for the rest of the coupons, which is expected due to the morphology on the different sides of the Nickel coupons, mentioned above. While investigating the Nickel coupons with the crevices perpendicular to the camera, the droplets tend to float out in the crevices causing oval shaped droplets and hence decreasing the contact angle significantly. On the other side, while investigating the droplets on crevices parallel to the camera, an increase of the contact angle is obvious. This, combined with the more realistic values on the mill oxide side of the coupon, is providing contact angles with large deviation. The values individually are deviant from the values expected from the surface treatment combined with the alloying elements, while the final result for the contact angles and SFE is very close to the expected values. The Nickel alloys does also provide similar results as the ones for Alloy 1 in regards to the value of the total SFE. All these alloys have been treated with the *low temperature - short time* and the dispersive contribution is furthermore equal to the total SFE of the coupon. The similarity in surface between these two alloys with totally different base materials is a interesting phenomenon. The SFE varies between different alloying grade combined with the nanomaterial surface treatment, proving the fact that the base material is independent of the final SFE. If the stainless steel, Alloy 1, is compared with the Nickel alloys regarding alloying grade of certain elements, there are similar amounts of Chromium in all of these alloys while the other alloying elements differ from each other. As being written about in the theory section, the Yttrium nanoparticles is enhancing the formation of Chromium rich oxides on the surface. This is causing the formation of Cr_2O_3 and Y_2O_3 to be equally devided, the surfaces are experiencing similar SFE since the total EWF for these surfaces are almost equal. The charge distribution does furthermore affect the electron fluctuation similarly.

When measuring the contact angles, due to the large amount of measurements, this was conducted during several different days. It was noticed that the droplets settled differently, in regards to change in angle and speed, between days. The lab in which the measurements were made, is relatively small and contains a few different instruments. The centrifuge, in particular, is the probable cause of a previously mentioned disturbance. This was distinguished approximately after one third of the measurements were made and because of this, the accuracy of some measurements are feasibly compromised by the vigorous shaking from the centrifuge.

4.5 Fouling Results

The result from the fouling test are mainly what connects the study to the practical application. For each inspection, particularly interesting results are presented. An overview of the submerged coupons from the first and second inspection is however to be found in Appendix B.

4.5.1 First Inspection

After having the coupons submerged for 20 days the first planned inspection was conducted. As expected, the bare sample of Alloy 4 had been the most affected since it not being stainless steel, Figure 4.11 (a). This sample stands out since it is the only coupon that shows any signs of corrosion. Not only does the bare Alloy 4 show signs of corrosion but has after these 20 days of submersion heavily formed corrosion products on the surface. Alloy 4 - Coating 4, Figure 4.11 (b), on the other hand exhibits some fouling on the edges of the coupon. In the picture, fouling material is on the main surface, but this growth does not adhere to all of the surface. The biofilm and subsequent growth actually only adheres to the edge of the coupon and lays on top of the surface due to the ascending from the subsea environment. Other than the addition of fouling, Alloy 4 - Coating 4 is visually unaffected by the subsea environment so far.

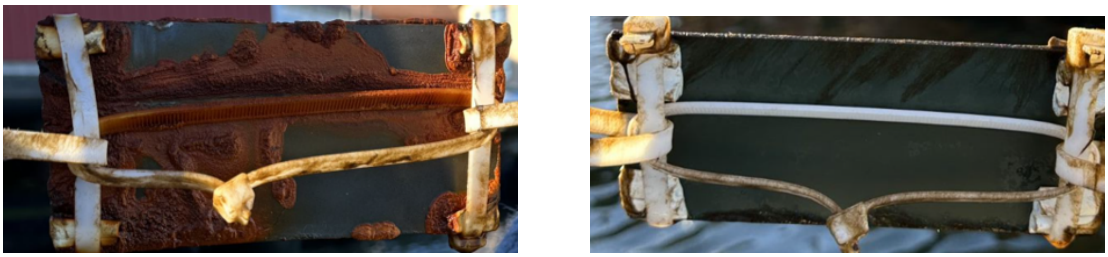

(a) **(b)**

Figure 4.11: Picture taken of (a) Alloy 4 - Bare and (b) Alloy 4 - Coating 4 after 20 days of submersion.

The coupon which showed the least amount of fouling after 20 days however is Alloy 1 - Coating 1, Figure 4.12 (a). There is no signs of corrosion as expected but also a very low amount of fouling. In Figure 4.12 (b) there is evidently fouling occurring at the edges, proving that it is the surface treatment that decreases the amount of fouling.

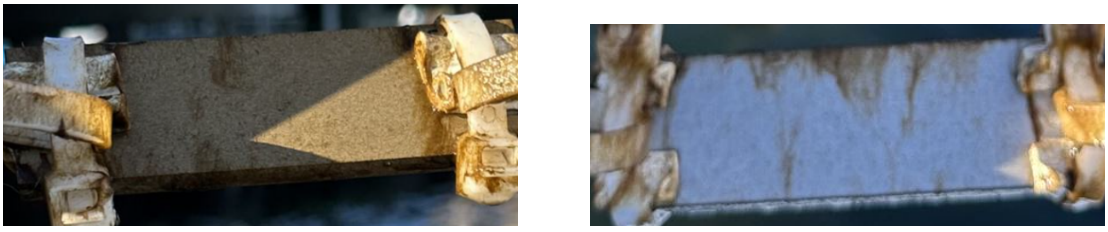

(a) **(b)**

Figure 4.12: Picture taken of (a) Alloy 1 - Coating 1 and (b) Alloy 1 - Bare after 20 days of submersion.

4.5.2 Second Inspection

After a total of 49 days from initial submersion, a second inspection took place. In Figure 4.13 (a), Alloy 1 - Coating 1 which had the minimum amount of fouling during the first inspection, however for the second inspection shows an increased amount of fouling, although seemingly mainly on the edge, although covering atop the relevant surface: somewhat impairing the evaluation. For Alloy 1 - Coating 2, Figure 4.13 (b), this is not the case. The little fouling that is present is clearly adhered mainly on the edge, as opposed to the bare Alloy 1 presented in Figure 4.13 (c).

(a) **(b)**

(c)

Figure 4.13: Picture taken of (a) Alloy 1 - Coating 1, (b) Alloy 1 - Coating 2, and (c) Alloy 1 - Bare after 49 days of submersion.

Another result showing low amounts of fouling is Alloy 2 - Coating 2, Figure 4.14 (a). Alike Alloy 1 - Coating 2 some fouling adheres to the relevant surface, but significantly less than the bare Alloy 2 coupon, Figure 4.14 (b).

(a) **(b)**

Figure 4.14: Picture taken of (a) Alloy 2 - Coating 2 and (b) Alloy 2 - Bare after 49 days of submersion.

4.5.3 Final Inspection and Completion

After a total of 76 days of submersion the fouling test was finalized and evaluated. In Table 4.10 the average values of the mass per surface area, ξ, are listed along with a ranking corresponding to which material system has the lowest average ξ. The average ξ was calculated from the values of ξ for each material system, presented in Appendix B, Table B.2. The copper based Alloy 5 has the lowest average ξ ans ranks number 1, followed by Alloy 1 (ranking 2-4, and 6) and 2 (ranking 5 and 7) with different coatings until ranking 8, which is Alloy 3 - Coating 2. Additionally, rank 2 through 10 are stainless steel alloys. Except for Alloy 5, the bare alloys have the highest average value of ξ ranking 16 to 18, where the regular carbon steel gets ranking 18.

The average ξ value for Alloy 5 is 0,00068 g/cm^2, which is roughly two thirds of Alloy 1 - Coating 2. However the individual ξ values for Alloy 5 is 0,0014 g/cm^2 and 0 g/cm^2, while the individual ξ values for Alloy 1 - Coating 2 is 0,0010 g/cm^2.

When focusing on one coating number at a time, it's clear that the stainless steel, Alloy 1, have superior values for each coating, consistently. Additionally, when focusing on one alloy number at a time, Coating 2 is top of the range.

Table 4.10: The average mass per surface area and their ranking.

Material System	Average ξ [g/cm^2]	Ranking
Alloy 5	0,00068	1
Alloy 1 - Coating 2	0,0010	2
Alloy 1 - Coating 4	0,0032	3
Alloy 1 - Coating 1	0,0034	4
Alloy 2 - Coating 2	0,0035	5
Alloy 1 - Coating 3	0,0035	6
Alloy 2 - Coating 4	0,0036	7
Alloy 3 - Coating 2	0,0036	8
Alloy 3 - Coating 3	0,0037	9
Alloy 2 - Coating 3	0,0038	10
Alloy 7 - Coating 1	0,0038	11
Alloy 2 - Coating 1	0,0048	12
Alloy 4 - Coating 4	0,0057	13
Alloy 3 - Coating 1	0,0060	14
Alloy 6 - Coating 1	0,0087	15
Alloy 2	0,016[a]	16
Alloy 1	0,016[a]	17
Alloy 4	0,026[a]	18

[a] one measurement made, not an average.

In Figure 4.15 (a), the copper based Alloy 5 is exhibiting clear signs of fouling, yet mainly originating from a specific place as opposed to the figures presented in previous Sections 4.5.1 and 4.5.2. On the contrary, the regular carbon steel, Alloy 4 Figure 4.15 (b), has obvious problems in regards to both fouling and corrosion.

(a) **(b)**

Figure 4.15: Picture taken of bare (a) Alloy 5 and (b) Alloy 4 after 76 days of submersion.

Since stainless steel Alloy 1 - Coating 2 is the material system with the lowest average ξ, after Alloy 5, it is presented along with its bare sample in Figure 4.16. The bare sample, Figure 4.16(b), has clear signs of fouling all over the surface as opposed to Coating 2, which does not have nearly as high amounts of fouling.

(a) **(b)**

Figure 4.16: Picture taken of (a) Alloy 1 - Coating 2 and (b) Alloy 1 - Bare after 76 days of submersion.

Continuing down the list in Table 4.10, Alloy 1 generally measured low ξ and in Figure 4.17 are the samples (a) Coating 4 and (b) Coating 1, with ranking 3 and 4, respectively.

(a) **(b)**

Figure 4.17: Picture taken of (a) Alloy 1 - Coating 4 and (b) Alloy 1 - Coating 1 after 76 days of submersion.

Lastly, in Figure 4.18, pictures of Alloy 2 - (a) Coating 1 and (b) bare, respectively, are presented.

(a) **(b)**

Figure 4.18: Picture taken of (a) Alloy 2 - Coating 2 and (b) Alloy 2 - Bare after 76 days of submersion.

It is clear that all coupons in Figure 4.15 to 4.18 have fouling on the surface. Although, it is not apparent which coupon has the most mass per surface area when it comes to the material systems in the middle range of the ranking presented in Table 4.10. The fouling on the surface is, as expected, not a homogeneous layer.

4.6 Fouling Test Discussion

From the first inspection it is apparent that the conditions are sufficient, where the regular carbon steel coupon, Alloy 4, has been experiencing severe corrosion attacks. After 76 days of submersion, the carbon steel alloy still stands out having high amounts of corrosion product and marine growth covering the surface. Carbon steel is the singular material system in this study that readily corrodes, which is expected due to its lack of corrosion resistant alloying elements. Additionally, carbon steel gained poor results regarding the fouling, inferior to the other material systems. However, carbon steel is the material system with second lowest SFE of the bare material systems. When investigating the ratio of the polar and dispersive contribution to the SFE, comparing the bare material systems, a trend becomes apparent. The polar contribution make up about 40% of the total SFE for the carbon steel while only 30% and 22% is the polar contribution to the bare stainless steels SFE, Alloy 1 and 2, respectively. Evidently, the polar contribution seems to have a more significant impact than the total SFE regarding fouling mitigating surfaces.

The indication that the surface treatments, Coating 1-3, are beneficial in regards to antifouling properties, was noticed already during the first inspection, in Figure 4.12. Since there is marine growth clearly manifested on the bare stainless steel coupon, but seemingly none on the surface treated coupons. Following, the second inspection indicates that some marine growth has adhered to the surface's of the stainless steels, Alloy 1 and 2, Figure 4.13 and 4.14, respectively. The coupons treated with Coating 2 experience small amounts of fouling for both Alloy 1 and 2, yet the bare coupons are subjected to significant amounts of marine fouling. When comparing the treated coupons with the bare one's for both Alloy 1 and 2 there is also a difference in type of the fouling. Marine biofilms are formed from a variety of bacteria which adhere to the surface with varying force and it is reasonable that some bacteria to not adhere at all to the surfaces with lower, or less polar, SFE. From inhibiting the formation of a biofilm, devastating consequences following MIC and pitting are avoided. Localized corrosion such as pitting is as mentioned a cause of unexpected and premature failure and is therefor of big concern regarding safety and hazard operations as well as economic return of investment.

Throughout the fouling test, but confirmed in the final inspection, the Copper based Alloy 5 is the material system which is proven superior. It is however the only bare material system that in any way challenges the surface treated stainless steel alloys. The second best bare material system is Alloy 2 closely followed by Alloy 1 which are also the third and second worst material system, respectively. The worst being regular carbon steel, Alloy 4 that is clearly unusable in subsea environments, mainly due to its insufficient corrosion resistance. Alloy 4 is not a material used in corrosive environments and was expected to generate the worst result in regards to corrosion, as mentioned. Alloy 1, on the other hand, is readily used in corrosive

environments which is reasonable since no apparent corrosion has formed on the surface. Although, it has 16 times as much mass from marine growth compered to when it has been treated with the *low temperature - long time surface treatment*, Coating 2. Alloy 1 - Coating 2 is the second best material according to Table 4.10 with an average ξ being almost twice the average value for Alloy 5. Although, the individual values for each coupon show that Alloy 1 - Coating 2 are more consistent than for Alloy 5. Copper alloy 5 has exceptionally small amounts of fouling mass per surface area: 0,0014 and 0 g/cm^2. Since previous research indicates that Copper based alloys have superior properties in subsea applications these values creates a good base for comparison. Furthermore, when comparing the individual values of Alloy 1 - Coating 2, both values are lower than one of the Copper alloy's values. Hence, it is reasonable to claim that Alloy 1 - Coating 2 could be as good as Alloy 5.

The SFE of a surface is known to have an effect on biofilm formation and fouling [5, 26, 30]. Yet, the two material systems having superior and similar results from the fouling test, Copper based Alloy 5 and surface treated stainless steel Alloy 1 - Coating 2, have deviating SFE values. The polar contribution to the Copper based alloy's total SFE is 20%, while the polar part is close to eliminated for the treated stainless steel. Then again, the total SFE for the treated stainless steel is 20% larger than the total SFE of the Copper based alloy. Evidently, the polar contribution to the SFE has a bigger impact on the fouling mitigating properties than the total SFE. This is previously claimed above when comparing the SFE and fouling results of the bare materials. Contradictory, the stainless steel alloy with the PTFE based paint coating, Alloy 1 - Coating 4, has an SFE value which is almost 75% of the treated stainless steel, Alloy 1 - Coating 2, but an average of fouling mass per area which is more than three times as large, although similar to the other surface treated stainless steels, see Table 4.10. Alloy 1 - Coating 2, which is the treated stainless steel with the lowest amount of mass per surface area does not have notably different SFE values compared to the other treated stainless steels. Therefore no direct conclusions can be drawn regarding specific material systems. However, the general trend manifested continuously throughout the discussion, is that the surface treatment eliminates the polar contribution to the SFE, which lowers the total SFE of the alloy. From eliminating the polar contribution, the material system resists marine fouling to the same extent as other material systems with greater polar contribution to their generally lower SFE value. There is also a difference between surface treatments, where the *low temperature - long time surface treatment*, Coating 2 continuously display superior results for the fouling test, Table 4.10. Evidently, a prolonged furnace exposure time positively affects the fouling mitigating properties. Longer thermal exposure is known to increase the thickness of TGO's which supports the conclusion that Coating 2 generates a thicker, less oxygen-permeable and feasibly more dense protective oxide.

The PTFE based coating on stainless steel, Alloy 1 - Coating 4, has proven to mitigate fouling to some extent in the fouling test. Alloy 1 - Coating 1 and 3 and Alloy 2 - Coating 2 have similar values as the stainless steels with Coating 4. Generally, Coating 2 displays good values, rank 2, 5, and 8 while Coating 4 have a broader range, rank 3, 7, and 13. It is interesting that Coating 4 has such a broad

range of results since the fouling should be independent on the base material. It is feasible that the lower ξ results of Coating 4, which are from the stainless steel Alloys 1 and 2, are in some way affected by the alloy itself, since only one side of the coupons are coated. This is however very unlikely since the bacteria surrounding the coupons are considered to be constant for each side of every coupon. Additionally, if that reasoning would apply, Alloy 4 coated with the PTFE based Coating 4 should be the coupon of which is the most representative of the PTFE based Coating 4, since it is fully coated like it would be when used during processing. It is however more likely that the surface roughness of the base material affects roughness of the coated surface. Contradicting this is the results that displays a larger improvement for Alloy 1 coated versus bare, than for Alloy 2. Nevertheless, the two alloys' results are generally similar, where individual variation of the samples could be the cause of this contradiction. Furthermore, there are general environmental problems following the use of coatings, presented previously in this report, Section 2.4. Coating 4 is however not a coating that leaches toxic chemicals, making the use of Coating 4 less concerning, compared to conventional paints used to reduce fouling. Still, paint particles, in other words microplastics, will still be released into the marine environment. By choosing to rather alter the surface of the material than to cover it, the previously mentioned problem can be eliminated. It is although important to make sure that new problems do not arise with this novelty surface treatment technology. However, the pre-treatment before the PTFE based Coating 4 is more extensive than the for the surface treatment, see Section 3.1.2.2. Further research of whether the surface treatment could benefit from pre-treating the surface is an aspect to keep in mind. Nevertheless, although pre-treatments and more advanced prepping methods than used in this study could be applied, it is clear that the surface treatment vastly improves the materials resistance to corrosion and marine fouling as is. Moreover, Coating 4 degrades when exposed to sunlight, UV-radiation, which is another concern using this coating. Although, the coating could be used in specific environments, the assembly becomes affected and the general applicability is limited.

Porosity and surface roughness affects the application of the nanomaterial based surface treatment as well as the antifouling properties of the material. It is known that biofilm formation is favored by a higher surface roughness [30], which is evident from the fouling test results. Clearly, even though the concentration of Yttrium is higher at the edge of the coupons, the bacterial development and marine fouling is primarily established at the edges. Concluding that there is a critical concentration of Yttrium that is important. Based on the SEM/EDX results, the structure of the coupon's surface is not affected by the surface treatment. Hence, it is reasonable to confirm that it is the change in composition following the surface treatment that affects the improvement in fouling mitigation of the material.

Based on the theory of MIC, a material that serves as an anode is more vulnerable to biofilm formation and MIC. This connects the corrosion resistance of a material to its fouling mitigating properties. This is supported by the fact that Alloy 1 compared to Alloy 2, which is less corrosion resistant, also have better results from the fouling test, treated and untreated. This is also evident when observing Alloy 4, which both readily corrodes and sustains the most marine growth on the

surface.

4.6.1 Subsequent Corrosion Analysis

In regards to the fouling test, the most interesting alloys and coatings were visually inspected according to their corrosion resistance. In figure 4.19, the best fouling resistant material system, Alloy 1 - Coating 2, except for the copper alloy is visualized beside its untreated counterpart. The alloys investigated should not experience severe corrosion attacks in only 76 days of submersion, which is clearly demonstrated. Although, the bare sample does experience some localized corrosion, which is thought to be pitting corrosion caused by MIC, on several locations all over the coupon. Even though the damages are minor, it can be considered a risk to use a non treated alloy of this kind since the submersion time, 76 days, is thought to be insufficient to cause severe pitting corrosion damages. The nanomaterial treated coupon, i.e. Alloy 1 - Coating 2, does not experience any of these corrosion attacks at all.

Figure 4.19: Alloy 1 - from left: Coating 2 submerged, Bare submerged, Bare

In Figure 4.20, the nanomaterial treated steel with the lowest alloying grade is being compared in regards to its different treatment parameters. For both the short time treatments, there is severe crevice corrosion present on the coupons, near the attachment locations for the cable ties and the rubber stripping, while the coupon treated for a longer time does not experience any visual corrosion damage at all. This is indicating that a longer heat treatment time could increase the corrosion resistance for coupons being treated with the nanocoating. Supporting the claim that the protective oxide gets thicker or more dense from prolonged thermal exposure, Coating 2, causing it to become less oxygen-permeable. This additionally negates the hypothesis that the change in parameters between surface treatments are negligible.

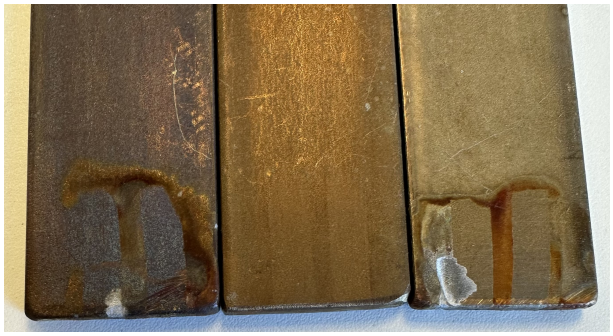

Figure 4.20: Alloy 2 Submerged - From left: Coating 3, Coating 2, Coating 1

As stated in the Theory section, the Copper alloy, Alloy 5, has been proved to perform impeccable in subsea environments, regarding its fouling mitigation and corrosion resistance. When comparing the coupons in Figure 4.21, no major difference in corrosion attacks are visual. Both coupons were outstanding in corrosion resistance during the 76 days of submersion. The visual difference between the coupons are obvious in regards to the exposed area. Alloy 5 is experiencing a tangible oxide growth, formation of CuO, which is enhancing the corrosion resistance. It also indicates that there is actual oxidation occurring on the surface according to the differences in shades on to the submerged coupon. Unlike the nanomaterial treated Alloy 1, which does not experience any additional visual oxidation. By these statements, the result supports the claim that the nanotreatment initiates the Reactive Element Effect on the treated surfaces and hence counteracting corrosion and further oxidation.

Figure 4.21: After submersion: Alloy 5 on top, Alloy 1 - Coating 2 on the bottom.

Additional comparison between the above stated coupons shows a minimal initiated local corrosion attack on Alloy 5, which is demonstrated in Figure 4.22. This could furthermore be compared and equated with the crevice corrosion attacks on Alloy 2 and Alloy 3 demonstrated in Figure 4.20, but in less extent. This indicates that the environment is indeed very harsch and the superiority of Coating 2 is obvious.

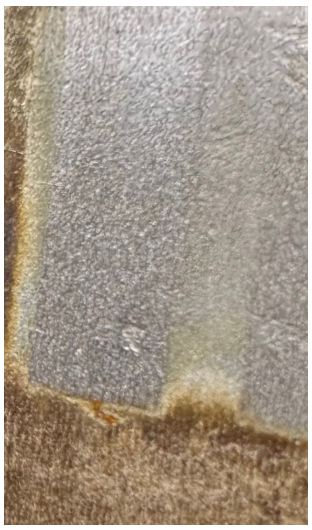

Figure 4.22: Small, visual, local corrosion attacks on Alloy 5.

4.7 Financial Aspects

If major fouling occurs on the surface on a subsea cooling station, the additional growth is going to affect its properties significantly. By adding a layer of marine growth onto the module it is going to affect the heat transfer caused by the natural convection. The more fouling that is present on the pipes, the more the heat transfer gets affected. Hence, the *heat transfer coefficient* or k-value is directly dependent on the thickness and amount of fouling present on the pipes' surface. An increase of the k-value does furthermore increase the efficiency of the cooler, and causing the OPEX to drastically increase due to additional maintenance costs. Another major parameter being affected by the fouling is furthermore the size of the cooler. The dimentions of the cooler are decided by the pipe length required to cool down the fluid inside the pipes by natural convection to the desired temperature. With more fouling present on the surface during fouling tests, a higher value for the *Fouling Factor,* U_f, is added to the simulations and design which results in longer pipe lengths and furthermore a larger subsea module to install to achieve the right amount of cooling. The fouling factor is furthermore defined as the inverse of the heat transfer coefficient.[65] Large amounts of fouling on the pipes are also affecting the flow rate of cooling water, in between the pipes, which is highly necessary to maintain the natural convection. Significant fouling would hence force the sizing to increase to counteract the decreased water flow between the pipes and maintain the right amount of cooling.

Material selections for subsea cooling design usually includes several expensive materials, in regards to piping materials and coatings, to fulfil the requirements stated in the previous section, and mitgate the amount of fouling. These materials should be able to maintain their structure and properties in a lifespan of everything in between 5 and 50 years. This requires materials with unique properties and a well developed protection system, which often results in a high CAPEX and low OPEX for the long lifespan projects without major maintenance. For the short lifespan, maintainable, projects the OPEX is usually increased while the CAPEX is decreased. For projects without planned maintenance, it is more critical to use materials known to be impeccable in these environments, but they do also tend to be extremely expensive. The high cost may cause some clients to reevaluate the product design and buy the concept from other companies, hence installing a product less safe or efficient causing the energy price for civilians to further increase over time since the product will not maintain efficient energy production.

The material systems in this study varies in price, but regarding to Table 2.6 and the results of the fouling test, the Yttrium based nanotreatment which is the most expensive material, is demonstrating superior results in combination with the highest alloyed stainless steel. It does almost experience the same amount of fouling as the Copper alloy, which is known to be a very fouling and corrosion resistant alloy.

Rare earth elements are known to be tough to mine, and very expensive, but yet a phenomenal alloying element. Even a tiny amount of rare earth elements in an alloy, about $1wt\%$, is causing the alloy to perform the REE while experiencing oxidizing environments. This is because the rare earth elements tend to move to

the surface to act as a protective barrier. If one wt% of Yttrium were added to the alloy for an entire cooling module, the CAPEX would increase significantly because of the prize of Yttrium, and an additional coating would be necessary to mitigate the fouling, since there is no change in the SFE upon addition of alloying elements. With the investigated nanotreatment, the Yttrium particles is dissolved in a solution evenly distributed and a size of approximately 5 nanometers each, and thus requires a much smaller amount of Yttrium to gain the rare earth metal alloying properties.

In accordance to these statments, it is possible to use rare earth elements to even minimize the CAPEX compared to traditional material systems by using this particular treatment. Since the properties of this nanotreatment, with certain treatment parameters in line with Coating 2, includes mitigation of fouling as well as great corrosion resistance, especially in combination with Alloy 1. Thus, it can be concluded that the OPEX cost could be decreased too. When adding all this up together, there is a high possibility that Alloy 1 - Coating 2 could perform as good as the well performing Alloy 5.

4.8 Ethical and Environmental Aspects

As mentioned previously, antifouling paint coatings have a negative impact on marine environments, both trough leaching and chipping of paint deposits. These coatings persist after their intended function, polluting the environment. By exploring alternative antifouling technologies, harmful technologies can eventually be phased out. The surface treatment investigated in this study is technically not a coating implying that waste would be prevented, but also does it not affect the heat transfer abilities of the application, according to the founder and producer of the product. Consequently creating a more efficient process which is important because there is then less energy and resources wasted during production. Maximizing efficiency in both fossil and renewable processes is an important step to ensure sustainability, emphasised by the *Swedish Environmental Protection Agency* [66]. Finding materials with superior antifouling properties and corrosion resistance will increase the efficiency of the application as well as require less maintenance. Moreover, maintenance is also interconnected with several risks regarding safety and environmental effects as well as it requires economic resources.

The copper based alloy investigated in this study, Alloy 5, is proven to have inherent resistance to marine growth. It has although been mentioned that copper in inherently toxic. However, approximately 90% of the piping in Sweden's household water supply system is made out of Copper based alloys and the concentration of Copper within the drinking water varies depending on water composition and residence time. Still, expected effects on health due to increased Copper concentration is considered to be low. [67] Copper is also naturally occuring in aquatic environments, although from the use of leaching paints, copper and other biocides have been shown to harm local marine environments. Also, when considering the size of the process equipment minimal leaching can still have a significant impact on the marine environment.

PTFE is a fluoropolymers and a *per- and polyfluoroalkyl substance*, PFAS. These substances are historically been used due to the stability caused by the Carbon-Fluor

bond, which is also the reason they degrade very slowly. PFAS's are thus bioaccumulating and many PFAS's are regulated within the EU. A proposal published in 2023 restricting the use of fluoropolymers, like PTFE, in all applications. [68] However, regardless of the regulations, Coating 4 does not compare to the investigated surface treatment.

Safety hazards caused by corrosion and MIC is another aspect to consider. Since all corrosion weakens the material, accidents can be avoided by using corrosion resistant and fouling mitigating materials. Malfunctions in industries have direct consequences both short and long term, permanently harming humans and society, as well as nature and the environment.

The rare earth element Yttrium is a fairly abundant element.[69] It is 26 000 times more common than gold, but there is yet a concern to meet global demand since it is used in many applications, such as flat panel screens and energy-efficient lighting. [69, 70] Yttrium can as mentioned be found in the mineral monazite as a by-product and Conventional mining processes generally require high energy and have a significant environmental impact. If the investigated surface treatment is to be implemented in future subsea processing equipment, the demand would increase. An increased demand could, from expanding the conventional mining process, cause further environmental impact and energy demand however, new and improved methods are already being investigated. A high demand can also serve as a catalyst for innovation, bringing about more energy efficient methods with a reduced environmental impact. [70]

5
Conclusion

This project has consisted of several parts, all equally contributing to the final statements and conclusions. The first part includes a theoretical investigation of possible oxidation and fouling mitigating parameters according to previous research and industrial experience. The second part includes physical testings of relevant and interesting material systems for oxidation and fouling mitigation. Novelty nanomaterial induced material systems has been investigated along with commonly used material systems in a comparasion study. The tests has mainly been treating the surface chemistry and properties of the material system to be aligned with a M.Sc in Materials Chemistry.

The final chapter of this project is treating the final statements and the results of the material testings is concluded. Limitations of the project are discussed to understand the extent this particular project has faced and how to improve it in further research. The discussion sections in the report is combined and the result of the discussions combined are demonstrated in a final material system to be the best option for subsea processing. Applications for the investigated surface treatment are demostrated along with further research opportunities for nanomaterials within subsea applications. To end the project, a short section about the culmination is added.

5.1 Limitations

Even though the studies were quite comprehensive, there are some limitations that needs to be taken into consideration when concluding the project. Two major limitation aspects are going to be taken into consideration for this particular project, with the first limitation being the *time* for the project. Since the Master Thesis only includes 30 credits, it had to be done in one semester or 20 weeks. Even though the fouling test were initiated quite early, the 76 days of submersion is not enough to establish a saturated amount of fouling. The visual inspections proved that the amount of fouling had been increasing between all visual inspections, causing the final fouling amount to be unsaturated, and hence not the final amount of fouling the subsea cooler station would experience in 50 years of operation.

The second relevant limitation to include is the *scope* of the project. When investigating the impact caused by the nanotreatment on the different coupons, a longer heat treatment time is improving the crucial subsea properties. This project describes only three heat treatment methods, where the *low temperature - long time* were considered to be the best option for subsea purposes. Nevertheless, the optimal heat treatment parameters for the nanotreatment is yet to be decided, since the gap between time and temperature for the different treatment methods is significant. Apart from the different treatment methods for the particular nanomaterial treatment, there are a few more interesting nanomaterial based coatings that could be of interest for the subsea market that this project do not cover. Hence, a conclusion whether this particular product is the optimal treatment for subsea coolers can not be drawn, even though the demonstrated results are impeccable.

5.2 Conclusion of the Results

The surface of the alloys have successfully been altered by adding a mixture containing nano-particles of Yttrium to the surface, enhancing the formation of a thin non-permeable protective oxide, containing both chromia and yttria. The rare earth element Yttrium causes the surface to become more oxygen reactive than scale forming, through the *reactive element effect*, thereby increasing the corrosion resistance. The information gathered from the EDX result indicates that it is the addition itself, rather than a higher concentration of Yttrium within the surface, that affects the SFE and hence also the fouling properties. All alloys that were treated with the nanoparticle surface treatment, Coating 1-3, experienced a change in SFE. The surface treatment decreases the SFE of the alloy, essentially by eliminating the polar contribution to the total SFE. The SFE of treated alloys' are subsequently established from the dispersive contribution of the SFE and affected by the alloys' composition, causing the final total SFE of each alloy to be alloy dependent. Although, the results of the SFE measurements are similar for Coating 1 through 3, the Fouling test highlights the superiority of the *low temperature - long time* treatment, Coating 2. Moreover, the mass from fouling per area for each alloy is continuously at its minimum following treatment of Coating 2. Thus, Coating 2 indicates results

which challenge conventional materials, in regards to corrosion and MIC resistance.

The material system of which showcase the least mass per area is the untreated Copper based Alloy 5, closely followed by the *low temperature - long time* treated stainless steel, Alloy 1 - Coating 2. The total SFE for the treated stainless steel is larger than the total SFE of the Copper based alloy which additionally has a larger polar contribution to the total SFE. Connecting the SFE and fouling results of several material systems it is argued that the polar distribution of the SFE effects fouling differently compared to the known phenomenon of a generally low total SFE inhibiting long term fouling. Additionally, Copper based alloys have been favoured historically in subsea applications, partly due to its toxicity. The *low temperature - long time* treated stainless steel material system, Alloy 1 - Coating 2, however does not pollute its local marine environments.

5.3 Applications

Up to date, within subsea processing, the use of biocidal materials has been the evident material selection for fouling mitigation for subsea coolers. This study contained several material system, with the target to challenge the commonly used, biocidal materials. The investigated nanomaterial surface treatment, which principally were founded to mitigate high temperature corrosion, has been proved to mitigate fouling to the same extent as the commonly used material in subsea processing. This can be concluded based on the test data presented in the results, Section (4), where a nanomaterial treated stainless steel is performing as good as the commonly used Copper based alloy in both regards to corrosion and fouling mitigation.

Rare earth elements are the cause for the designation "superalloys", when being added to an alloy in a small concentration. The prize for inducing rare earth elements to an alloy is not yet beneficial for industries, since rare earth elements are very expensive, even in small concentrations. This technique, however, is allowing for a nanoscale amount of rare earth elements to behave as well as a commonly known rare earth induced superalloys, by manipulating the chemical composition of a given metallic surface.

Nanoparticles have not previously been used in subsea processing to a large extent. However, it is becoming more commonly spoken about because of its impeccable properties regarding oxidation resistance in combination with the opportunity to modify surface properties. This study within nanomaterial surface treatments could create additional paths within nanomaterial engineering to develop material systems compatible with offshore engineering.

5.4 Culmination

The novelty surface treatment investigated in this study has proven to effectively enhance the fouling mitigating properties and the corrosion resistivity of stainless steels

and nickel based alloys. Furthermore, Coating 2 could potentially be an alternative to possibly lower the CAPEX of traditional material systems while maintaining a low OPEX, since relatively low amounts of Yttrium is used and the lifetime of the application is heavily extended compared to commonly used coating systems. Presented in this study is a material system that has been proven to challenge the established materials currently available and used within subsea processing.

Bibliography

[1] Crash Course. Humans and energy: Crash course world history 207. Video, Aug 2014. url: https://www.youtube.com/watch?v=EM1IyIyr-Zc.

[2] Amanda Onion, Missy Sullivan, Matt Mullen, and Christian Zapata. Website, April 2010. Last updated: March 2023. url: https://www.history.com/topics/industrial-revolution/oil-industry.

[3] W.T. Lie, W. Tang, and X. Xie. Wind power distribution over the ocean. *Geophysical Research Letters*, 35, 2008.

[4] Lienau Bernd. Subsea cooling system for offshore wind. *Technical Disclosure Commons*, 2022.

[5] Maureen E. Callow and Robert L. Fletcher. The influence of low surface energy materials on bioadhesion — a review. *International Biodeterioration & Biodegradation*, 34(3):333–348, 1994. Special Issue Marine Biofouling and Corrosion.

[6] J. H. L. Voncken. The rare earth elements—a special group of metals. In *The Rare Earth Elements: An Introduction*, pages 1–13. Springer International Publishing, Cham, 2016.

[7] Volker Zepf. Rare earth elements: What and where they are. In *Rare Earth Elements: A New Approach to the Nexus of Supply, Demand and Use: Exemplified along the Use of Neodymium in Permanent Magnets*, pages 11–39. Springer Berlin Heidelberg, Berlin, Heidelberg, 2013.

[8] Gordon B. Haxel, James B. Hendrick, and Greta J. Orris. Rare earth elements - critical resources for high technology, 2005. U.S. Geological Survey.

[9] Guodong Wang, Meng Fan, and Wenqing Liu. Effects of yttrium on the microstructure and properties of aluminum alloys: A review. *Materials*, 12(23), 2019.

[10] Maria Forsyth and B.R.W. Hinton. Rare earth-based corrosion inhibitors. pages 1–319, 01 2014.

[11] P.Y. Hou. The reactive element effect – past, present and future. *Materials Science Forum*, 696:39–44, 09 2011.

[12] C Avci, R Yilmaz, and M Ata. Rare earth elements and their effect on materials properties. *International Journal of Materials Science and Applications*, 6(6):299–304, 2017.

[13] Jonathan Ayutsede, Susan Kerber, Ed Curran, Brandon Dooley, Ian Luna, and Les Jackowski. Novel Surface Treatment to Mitgate Fouling in Heat Exchangers and Process Equipment. Technical report.

[14] Xiaolian Liu et. al. Title of the article. *Materials Research Express*, 10(2):1–11, 2023.

[15] Britannica. work function, 2023. Accessed on March 27, 2023.

[16] Richard G. Forbes. *What do We Mean by Work Function" ?*, pages 163–172. Springer Netherlands, Dordrecht, 1990.

[17] John Harris, Chih-Ting Chen, and John Wacker. Work function values for clean metallic elements: An experimental determination and discussion of the results. *Surface Science*, 540(2-3):253–269, 2003.

[18] Bengt Kronberg, Krister Holmberg, and Björn Lindman. *Wetting and Wetting Agents, Hydrophobization and Hydrophobizing Agents*, chapter 20, pages 377–390. John Wiley & Sons, Incorporated, 1st edition, 2014.

[19] Kruss Scientific. Surface free energy. Website, Accessed 2023. url: https://www.kruss-scientific.com/en/know-how/glossary/surface-free-energy.

[20] Brighton Science. What is the difference between surface free energy and surface energy? Website, September 2021. Accessed on 29 March 2023. url: https://www.brighton-science.com/blog/what-is-the-difference-between-surface-free-energy-and-surface-energy.

[21] Annamalai, Gopinadhan, Han, Saha, Park, Kumar, Patra, Kim, and Venkatesan. Surface energy and wettability of van der waals structures. *The Royal Society of Chemistry 2016*, 2015.

[22] Attension. Surface free energy - theory and calculations. Technical report, Biolin Scientific. url: https://cdn2.hubspot.net/hubfs/516902/Pdf/Attension/Tech%20Notes/AT-TN-04-Surface-free-energy-theory.pdf.

[23] Christine Bressy and Marlène Lejars. Marine Fouling An Overview. *The Journal of Ocean Technology*, 9(4):19–28, 2014.

[24] E. Nebot, J F Casanueva, R Solera, C Pendón, L J Taracido, T Casanueva-Robles, and C López-Galindo. Marine Biofouling in Heat Exchangers. In Jun Chan and Shing Wong, editors, *Biofouling: Types, Impact and Anti-Fouling*, chapter 3, pages 1–40. Nova Science Publishers, Inc., 2010.

[25] Ajay K Singh. Introduction to corrosion. In *SpringerBriefs in Materials*, chapter 1, pages 1–25. Springer Nature Singapore, Singapore, 2020.

[26] Ajay K Singh. Microbial induced corrosion and related theories. In *SpringerBriefs in Materials*, chapter 2, pages 26–43. Springer Nature Singapore, Singapore, 2020.

[27] Andrzej Kuklinski and Wolfgang Sand. Microbiologically influenced corrosion. In Gerhard Kreysa, Ken-ichiro Ota, and Robert F. Savinell, editors, *Encyclopedia of Applied Electrochemistry*, pages 1276–1290. Springer New York, New York, NY, 2014.

[28] Reza Javaherdashti. Corrosion and biofilm. In *Biofilm and Materials Science*, pages 69–78. Springer International Publishing, 1 2015. doi: 10.1007/978-3-319-14565-5_9 ISBN:9783319145655.

[29] Mirul K. Pal and M. Lavanya. Microbial influenced corrosion: Understanding bioadhesion and biofilm formation. *Journal of Bio- and Tribo-Corrosion*, 8, June 2022.

[30] Ajay K Singh. Industrial cases of microbial induced corrosion. In *SpringerBriefs in Materials*, chapter 5, pages 81–106. Springer Nature Singapore, Singapore, 2020.

[31] L Vedaprakash, P Senthilkumar, D Inbakandan, and R. Venkatesan. Marine Biofouling and Corrosion on Long-Term Behavior of Marine Structures. In *A Treatise on Corrosion Science, Engineering and Technology*, pages 447–466. Springer Singapore, 2022.

[32] Takaomi Arai, Hiroya Harino, Madoka Ohji, and William John Langston, editors. *Ecotoxicology of Antifouling Biocides*. Springer Science and Business Media, 2009.

[33] Andrew Turner. Marine pollution from antifouling paint particles. *Marine Pollution Bulletin*, 60:159–171, 2 2010.

[34] International Labour Organization. ICSC 0240 - COPPER, 2016. Last accessed 16 February 2023.

[35] Wenrui Dong, Bucheng Li, Jinfei Wei, Ning Tian, Weidong Liang, and Junping Zhang. Environmentally friendly, durable and transparent anti-fouling coatings applicable onto various substrates. *Journal of Colloid and Interface Science*, 591:429–439, 6 2021. doi: 10.1016/j.jcis.2021.02.014, ISSN: 10957103.

[36] Andrew Turner. Paint particles in the marine environment: An overlooked component of microplastics. *Water Research X*, 12, July 2021. doi: https://doi.org/10.1016/j.wroa.2021.100110.

[37] Ulla Ehrnstén, Leena Carpén, and Kimmo Tompuri. Microbially induced corrosion in firefighting systems—experience and remedies. In John H. Jackson, Denise Paraventi, and Michael Wright, editors, *Proceedings of the 18th International Conference on Environmental Degradation of Materials in Nuclear Power Systems – Water Reactors*, pages 2047–2056. Springer International Publishing, Cham, 2019. ISBN: 978-3-030-04639-2.

[38] Ajay K Singh. Microbial induced corrosion and industrial economy. In *SpringerBriefs in Materials*, chapter 3, pages 45–55. Springer Nature Singapore, Singapore, 2020.

[39] Jean-Pierre Celis. Austenitic stainless steels in subsea environments. *Materials and Corrosion*, 63(7):581–590, 2012.

[40] PF Zweifel and JE Schaffer. Duplex stainless steels for subsea applications. In *Proceedings of the 2001 Offshore Technology Conference*. Offshore Technology Conference, 2001.

[41] Australian Stainless Steel Development Association. Corrosion resistance of stainless steels, n.d.

[42] G. Gunasekaran, S. Rajakumar, and N. Arivazhagan. Duplex stainless steel - an overview. *ScienceDirect*, 2018.

[43] Nalco. Copper alloys. In *Nalco Guide to Cooling Water Systems Failure Analysis*, chapter 4. McGraw-Hill Education, New York, 2nd edition, 2015.

[44] Georges Valette. Hydrophilicity of metal surfaces: Silver, gold and copper electrodes. *Journal of Electroanalytical Chemistry and Interfacial Electrochemistry*, 139(2):285–301, 1982. doi: https://doi.org/10.1016/0022-0728(82)85127-9.

[45] Pierre R. Roberge. Engineering materials. In *Handbook of Corrosion Engineering*, chapter 11.6. McGraw-Hill Education, New York, 3rd edition, 2019. url: https://www.accessengineeringlibrary.com/content/book/9781260116977/toc-chapter/chapter11/section/section38.

[46] George S. Brady, Henry H. Clauser, and John A. Vaccari. Part 1 in materials, their properties and uses (a - e). In *Handbook: An Encyclopedia for Managers, Technical Professionals, Purchasing and Production Managers, Technicians, and Supervisors*. McGraw-Hill, New York, 15th edition, 2002. url: https://www.accessengineeringlibrary.com/content/book/9780071360760/chapter/chapter1.

[47] James H. Michel, Carol A. Powell, and Harold T. Michels. An assessment of the biofouling resistance and copper release rate of 90-10 copper-nickel alloy. In *Corrosion 2011*, Paper 11352. NACE nternational, March 2011. url: https://www.copper.org/applications/marine/cuni/pdf/11352exNACECD.pdf.

[48] Copper Development Association Inc. Environmental properties. Website, Accessed 10 May 2023. url: https://copper.org/applications/marine/cuni/properties/environmental/.

[49] Raul B. Rebak and Paul Crook. Nickel alloys for corrosive environments. *Advanced Materials & Processes*, 157(2):37, Feb 2000.

[50] John H. Thunderman. Nonferrous metals and alloys; metallic specialties. In Ali M. Sadegh and William M. Worek, editors, *Marks' Standard Handbook for Mechanical Engineers*, chapter 4.4. McGraw-Hill Education, New York, 12th edition, 2018. url: https://www.accessengineeringlibrary.com/content/book/9781259588501/toc-chapter/chapter4/section/section33.

[51] Jr. Sheldon W. Dean, Vinay P. Deodeshmukh, Emory A. Ford, James D. Fritz, Kevin L. Ganschow, Jr. Lindell R. Hurst, Pradip R. Khaladkar, Paul E. Manning, Edward R. Naylor, Richard C. Sutherlin, and Eugene L. Liening. Nonmetallic materials for corrosion control. In Don W. Green and Marylee Z. Southard, editors, *Perry's Chemical Engineers' Handbook*, chapter 25.12. McGraw-Hill Education, New York, 9th edition, 2019.

[52] Wesley Lock Sulen, Kesavan Ravi, Chrystelle Bernard, Yuji Ichikawa, and Kazuhiro Ogawa. Deposition mechanism analysis of cold-sprayed fluoropolymer coatings and its wettability evaluation. *Journal of Thermal Spray Technology*, 29:1643–1659, June 2020. doi: https://doi.org/10.1007/s11666-020-01059-w.

[53] Uta Klement. Thermal barrier coatings. Lecture slides, Chalmers School of Technology, 2022.

[54] Britannica Academic. Rare-earth element. Website, Jan 2019. Accessed 19 Apr. 2023. url: https://academic-eb-com.eu1.proxy.openathens.net/levels/collegiate/article/rare-earth-element/110615.

[55] S. R. Paital and P. Sahoo. Influence of yttrium addition on corrosion behavior of stainless steel. *Journal of Rare Earths*, 32(7):631–636, July 2014.

[56] Ruben Perez and Adam Hannon. Cleaning and preparation of electron optical instrumentation. *Microscopy Today*, 18(3):12–18, 2010.

[57] Mark A. Atwater. Property-based classifications of metals. In *Materials and Manufacturing: An Introduction to How They Work and Why It Matters*, chapter 4.4. McGraw-Hill Education, New York, 1st edition, 2019. url: https://www.accessengineeringlibrary.com/content/book/9781260122312/toc-chapter/chapter4/section/section40.

[58] James Chen. Troye ounce: Definition, history, and conversion table. Website: Investopedia, Febuary 2023. Cited March 2023. url: https://www.investopedia.com/terms/t/troyounce.asp.

[59] Leon Becker. Chemical elements by market price. Website, Oct 2018. Accessed April 2023. url: http://www.leonland.de/elements_by_price/en/list.

[60] Nanoscience Instruments. Attension theta lite. https://www.nanoscience.com/products/optical_tensiometers/attension-theta-lite/, March 2023.

[61] Nanoscience Instruments. One attension software for all tensiometry and contact angle measurements. https://www.nanoscience.com/products/one-attension-software-for-all-tensiometry-and-contact-angle-measurements/, March 2023.

[62] Britas Klemens Eriksson, Lena Rubensdotter, Eli Rinde, Stian Huseby, Fredrik Sundqvist, and Ali Buriyo. Macroalgae biomass in the deep waters of the Gullmar fjord, Sweden. *Journal of Environmental Science and Health, Part A*, 53(3):220–227, 2018.

[63] Python Software Foundation. Python^{TM}. https://www.python.org/, 2023.

[64] Chen Chen, Haiyang Zhan, Xiangge Bai, Zichao Yuan, Lei Zhao, Yahua Liu, and Shile Feng. Bionic superhydrophobic surfaces based on topography of copper oxides. *Biosurface and Biotribology*, 8(3):199–211, 2022.

[65] John E. Hesselgreaves, Richard Law, and David A. Reay. Compact heat exchangers in practice. 2016.

[66] The Swedish Environmental Protection Agency. Klimatet och energin. Website, Accessed March 2023. url: https://www.naturvardsverket.se/amnesomraden/klimatomstallningen/omraden/klimatet-och-energin/.

[67] Mia Kristersson, Emma Halldin Ankarberg, Sanna Lignell, Åsa Rosengren, Christina Lantz, and Emma Hansson. Metaller i kontakt med livsmedel riskhanteringsrapport. Technical report, Livsmedelsverket, 2017. ISSN: 1104-7089.

[68] chemsec. PFAS Guide. Website, Accessed 9 May 2023. url: https://pfas.chemsec.org/?gclid=CjwKCAjw3ueiBhBmEiwA4BhspMAtAmgeW5pYVusQFR2Onsr2P6AdHwo5CN1HGXdxjpW1yCv-dA-BRRoCjtQQAvD_BwE#regulation.

[69] Chin Trento. Main applications of yttrium in alloys and phosphors. Website, Accessed 10 May 2023. url: https://www.samaterials.com/main-applications-of-yttrium-in-alloys-and-phosphors.html.

[70] Carolina Mocelin Gomes Pires, Haroldo de Araújo Ponte, Jucélio Tomás Pereira, and Maria José Jerônimo de Santana Ponte. Yttrium extraction from soils by electric field assisted mining applying the evolutionary operation technique. *Journal of Cleaner Production*, 227:272–279, 2019. orl: https://www.sciencedirect.com/science/article/pii/S0959652619311552.

A

Appendix

CONFIDENTIAL

B

Appendix

B.1 Fouling Module

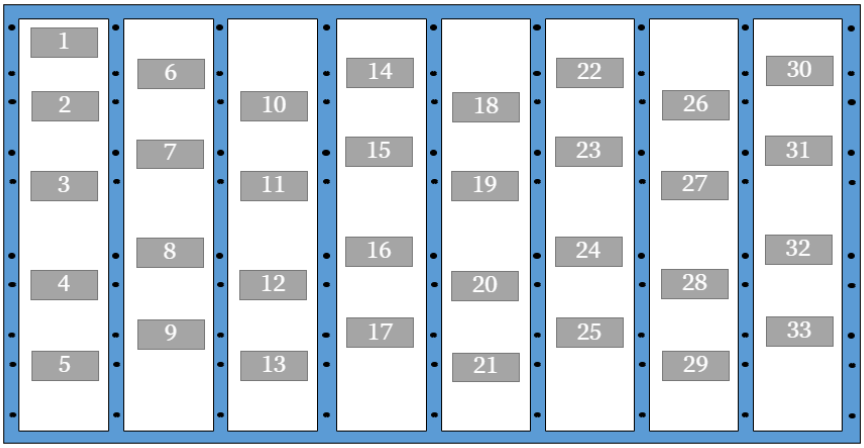

Figure B.1: Illustration of the subsea module used in the antifouling test

Table B.1: Sample positions of the antifouling test

1 - Alloy 6	12 - Alloy 1, Coating 3	23 - Alloy 2, Coating 3
2 - Alloy 2	13 - Alloy 4, Coating 4	24 - Alloy 1, Coating 4
3 - Alloy 5	14 - Alloy 1, Coating 4	25 - Alloy 6
4 - Alloy 3, Coating 3	15 - Alloy 2, Coating 4	26 - Alloy 2, Coating 2
5 - Alloy 1, Coating 3	16 - Alloy 5	27 - Alloy 3, Coating 3
6 - Alloy 4	17 - Alloy 3, Coating 1	28 - Alloy 1, Coating 1
7 - Alloy 7	18 - Alloy 2, Coating 3	29 - Alloy 3, Coating 2
8 - Alloy 2, Coating 4	19 - Alloy 7	30 - Alloy 3, Coating 2
9 - Alloy 1	20 - Alloy 1, Coating 2	31 - Alloy 4, Coating 4
10 - Alloy 1, Coating 1	21 - Alloy 3, Coating 1	32 - Alloy 2, Coating 1
11 - Alloy 2, Coating 2	22 - Alloy 2, Coating 1	33 - Alloy 1, Coating 2

B.2 Fouling Test Images

Presented below in Figure B.2 are the subsea module (a) during the first inspection and (b) during the second inspection.

(a)

(b)

Figure B.2: Picture of the subsea module at the (a) first inspection and (b) second inspection.

B.3 Fouling Raw Data

The raw data collected during the final inspection of the fouling test is presented in Table B.2. In the rightmost column is the ranking which corresponds to amount of mass per surface area. The coupon of the copper based Alloy 5 has, in this table, ranking 0 since there is no mass per surface area and ranking 1 goes to the coupon with the least amount of mass per surface area, stainless steel Alloy 1 - Coating 2. Following this logic, ranking 32 has the most amount of mass per surface area, regular steel Alloy 4.

Table B.2: Raw data collected, the calculated mass per surface and their ranking collected during the final inspection of the Fouling test.

Alloy no.	**Coating no.**	m_0 [g]	m [g]	A [cm^2]	ξ [g/cm^2]	**Ranking**
1	-	1,68	1,79	6,70	0,016	31
2	-	1,70	1,82	7,65	0,016	30
4	-	1,70	1,88	7,02	0,026	32
5	-	1,70	1,70	14,70	0,00	0
5	-	1,69	1,71	14,70	0,0014	4
1	1	1,71	1,72	9,52	0,0011	3
1	1	1,70	1,74	6,88	0,0058	25
2	1	1,69	1,73	9,90	0,0040	18
2	1	1,69	1,75	10,98	0,0055	23
3	1	1,69	1,72	10,07	0,0030	10
3	1	1,71	1,81	11,02	0,0091	28
6	1	1,70	1,76	8,16	0,0074	26
6	1	1,69	1,76	6,90	0,010	29
7	1	1,71	1,74	8,00	0,0038	14
7	1	1,70	1,73	7,79	0,0039	16
1	2	1,7	1,72	20,70	0,00097	1
1	2	1,70	1,72	19,50	0,0010	2
2	2	1,70	1,72	8,80	0,0023	8
2	2	1,68	1,71	6,40	0,0047	21
3	2	1,69	1,71	9,50	0,0021	6
3	2	1,71	1,75	7,80	0,0051	22
1	3	1,68	1,70	6,44	0,0031	11
1	3	1,68	1,71	7,70	0,0039	17
2	3	1,70	1,72	10,08	0,0020	5
2	3	1,70	1,75	9,00	0,0056	24
3	3	1,70	1,73	10,64	0,0028	9
3	3	1,67	1,70	6,63	0,0045	20
1	4	1,70	1,72	9,12	0,0022	7
1	4	1,72	1,77	12,00	0,0042	19
2	4	1,68	1,71	8,50	0,0035	12
2	4	1,67	1,70	8,12	0,0037	13
4	4	1,67	1,70	7,99	0,0038	15
4	4	1,70	1,75	6,60	0,0076	27

C

Appendix

In Appendix C, more detailed results for the contact angles and surface energies is displayed. The python code generated for solving the system of equations 2.7 is also displayed.

C.1 Surface Energy Calculations

C.2 Python Code

```
from sympy import symbols, Eq, solve, Abs
import math

# Constants
Lv1 = 72.8 #Surface tension of Water
Lv2 = 43.5 #Surface tension of DMSO
LVD1 = 22.8 #Dispersive part Water
LVD2 = 34.8 #Dispersive part DMSO
LVP1 = 50.0 #Polar part Water
LVP2 = 8.7 #Polar part DMSO

# Contact Angles
theta1_degrees = XX #Water
theta2_degrees = YY #DMSO

# Convert to radians
theta1 = math.radians(theta1_degrees)
theta2 = math.radians(theta2_degrees)

# Define variables
x, y = symbols('x y', real=True)

# System of equations
eq1_pos = Eq(0.5 * Lv1 * (1 + math.cos(theta1))
- (x*LVD1)**0.5 + (y*LVP1)**0.5, 0)
eq1_neg = Eq(0.5 * Lv1 * (1 + math.cos(theta1))
- (x*LVD1)**0.5 - (y*LVP1)**0.5, 0)
eq2_pos = Eq(0.5 * Lv2 * (1 + math.cos(theta2))
- (x*LVD2)**0.5 + (y*LVP2)**0.5, 0)
eq2_neg = Eq(0.5 * Lv2 * (1 + math.cos(theta2))
- (x*LVD2)**0.5 - (y*LVP2)**0.5, 0)

# Solve the equations
try:
    sol_pos = solve((eq1_pos, eq2_pos), (x, y), complex=True)
    sol_neg = solve((eq1_neg, eq2_neg), (x, y), complex=True)
    sol = sol_pos + sol_neg
    print(sol)
except ValueError:
    print("The system of equations does not have any real solutions.")
```

```
for s in sol:
    x_value = s[0].evalf()
    y_value = s[1].evalf()

    Sln = s[0].evalf() + s[1].evalf()
    print(f"Dispersive: {x_value} mN/m,
    Polar: {y_value} mN/m, Total SFE is {Sln} mN/m")

# Error handling for invalid input values
if Lv1 <= 0 or Lv2 <= 0 or LVD1 <= 0 or LVD2 <= 0 or LVP1 <= 0:
    print("Error: Surface tensions and
    dispersive/polar parts must be greater than 0.")
elif theta1_degrees < 0 or theta1_degrees > 180 or
theta2_degrees < 0 or theta2_degrees > 180:
    print("Error: Contact angles must be between 0 and 180 degrees.")
else:
    # Valid input values, proceed with calculations
    pass
```

D

Appendix

D.1 EDX data

No peak was found indicating the presence of Yttrium, therefore the EDX analysis does not include it for Alloy 1 - Bare. In Figure 4.1 (b), spectra 4 and 5 are located upon two different aggregates while spectra 2 and 3 are located generally on the surface. When comparing this to the values in Table D.1 the conclusion can be drawn that the aggregates experience a higher concentration of Yttrium. In spectrum 4, the amount of Oxygen is considerably greater than for surrounding spectras while the amount of Chromium, Iron, Nickel, and Molybdenum has decreased. The amount of Carbon is similar in each spectra of Coating 1, 2 and 3 and there is generally higher amounts of Carbon on the bare Alloy 1. Observing spectra 1 and 3 for Coating 2 and 3, the trend of increased Oxygen levels alongside increased Yttrium levels within the aggregates is apparent. However, the amount of Chromium seems to increase in the aggregates of Coating 2 while for Coating 3 it do not follow any pattern. The concentration of Iron and Nickel are both smaller in the aggregates for Coating 2 and 3, unlike the case for Coating 1. Molybdenum levels also increases in the aggregates for Coating 3 but its trend for Coating 2 is inconclusive.

Table D.1: Weight percentages of the main elements in Alloy 1: Bare, Coating 1, 2, and 3. Analysed using EDX.

Spectrum Alloy 1 - Bare	**C**	**O**	**Cr**	**Fe**	**Ni**	**Y**	**Mo**	**Other**
1	8,01	2,38	18,44	58,12	7,37	-	3,75	1,93
2	11,76	2	18,75	55,3	7,44	-	3,3	1,45
3	11,67	1,67	19,21	55,71	7,22	-	3,02	1,50
4	6,14	0,65	21,5	59,44	7,29	-	3,85	1,13
5	8,96	0,98	22,04	56,72	6,09	-	4,04	1,17
6	11,05	1,04	21,19	55,64	6,16	-	3,56	1,36
Alloy 1 - Coating 1								
2	1,65	1,42	18,54	61,74	12,68	0,37	2,97	0,63
3	1,43	1,97	18,18	62,59	11,35	0,57	3,31	0,60
4	2,74	23,07	14,19	45,05	1,79	2,3	0,58	10,28
5	2,42	2,88	18,74	60,13	11,31	1,17	2,58	0,77
Alloy 1 - Coating 2								
1	2,85	10,89	21,71	48,68	9,7	2,5	2,19	1,48
2	2,12	1,69	18,97	62,41	11,52	0,2	2,29	0,80
3	5,06	36	22,87	26,33	4,2	3,01	1	1,53
Alloy 1 - Coating 3								
1	4,03	43,88	9,96	32,24	3,22	4,29	1,07	1,31
2	1,96	3,73	17,32	58,71	10,94	3,35	3,2	0,79
3	3,45	18,26	20,56	38,17	5,65	10,76	1,85	1,3

The values for Alloy 2, presented in Table D.2, can not be directly compared to the values for Alloy 1 and 3. Because only Oxygen, Chromium and Yttrium are analysed for Alloy 2 - Coating 1 the weight percentages are higher than when more

elements are considered. To combat this, the calculated mean is the corresponding values for the bare sample, only considering Oxygen and Chromium. It's then shown that the chromium amount has decreased in all spectra, with larger decrease when the Yttrium increase is larger. This follows the trend found for Alloy 1 coating 1, spectrum 4, Table D.1. However, the increase of Oxygen is largest when the increase of Yttrium is lowest, which contradicts the trend shown for Alloy 1 - Coating 1. Furthermore, the amount of Oxygen are similar to that of the bare sample in the spectra where Yttrium is most abundant.

Table D.2: Weight percentages of the main elements in Alloy 2 - Bare and weight percentages of Oxygen, Chromium, and Yttrium in Alloy 2 - Coating 1, generated using EDX. Additionally, a calculated mean excluding all elements but Oxygen and Chromium for Alloy 2 - Bare.

Spectrum Alloy 2 - Bare	**C**	**O**	**Cr**	**Fe**	**Ni**	**Y**	**Mo**	**Other**
1	15,76	2,51	14,72	56,05	8,04	-	1,5	1,42
2	9,49	1,57	15,85	60,91	8,98	-	1,66	1,54
3	16,6	3	14,78	55,05	7,75	-	1,36	1,46
Calculated mean	-	*13,50*	*86,50*	-	-	-	-	*0*
Alloy 2 - Coating 1								
1	-	16,98	80,09	-	-	2,93	-	0
2	-	12,93	76,65	-	-	10,42	-	0
3	-	14,63	69	-	-	16,38	-	-0,01

The Yttrium values for Alloy 1 - Coating 1 and 2 are alike Alloy 3 Coating 1 when comparing the EDX analysis. Similarily, trends like Oxygen increasing and Chromium and Iron decreasing with higher Yttrium percentages can be noticed for Alloy 3.

Table D.3: Weight percentages of the main elements in Alloy 3 - Bare and weight percentages of Oxygen, Chromium, and Yttrium in Alloy 3 - Coating 1, generated using EDX.

Spectrum Alloy 3 - Bare	**C**	**O**	**Cr**	**Fe**	**Ni**	**Y**	**Other**
1	3,60	0,60	17,09	67,04	9,84	-	1,83
2	3,36	0,51	16,75	67,63	9,89	-	1,86
3	0,47	0,03	19,47	71,46	7,19	-	1,38
Alloy 3 - Coating 1							
1	7,22	6,11	15,2	53,87	6,58	2,54	8,48
2	2,43	1,47	16,59	66,37	9,85	1,35	1,94
3	0,9	0,52	17,89	70,16	8,6	0,5	1,43

The in the column "Other" all values are below two weight percent, except two

where the values are close to ten weight percent. This is unsettling, although has a simple explanation. The first high other value of 10,28 is driven up by a measured weight percentage of Silicon being 9,17 while the second other value of 8,48 comes from measuring 6,17 weight percent of Sulfur. The measurements of Silicone and Sulfur has consistently been below one weight percent for the considered alloy. These outliers can be explained to be caused by the phenomenon of when analysing minor trace elements of low atomic number, poor distinction of different elements from overlapping spectral peaks and background causing errors in the identification [1,2].

Bibliography

Appendix D.

[1] Deena Titus, E. James Jebaseelan Samuel, and Selvaraj Mohana Roopan. Nanoparticle characterization techniques. In *Ashutosh Kumar Shukla and Siavash Iravani*, editors, Green Synthesis, Characterization and Applications of Nanoparticles, Micro and Nano Technologies, chapter 12, pages 303–319. Elsevier, 2019. ISBN:978-0-08-102579-6 doi: https://doi.org/10.1016/B978-0-08-102579-6.00012-5 url: https://www.sciencedirect.com/science/article/pii/B9780081025796000125.

[2] J.S. Heslop-Harrison. Energy dispersive x-ray analysis. In *Physical Methods in Plant Sciences*, pages 244–277. Springer-Verlag Berlin, Heidelberg, 1990.

DEPARTMENT OF APPLIED CHEMISTRY
CHALMERS UNIVERSITY OF TECHNOLOGY
Gothenburg, Sweden
www.chalmers.se

CHALMERS
UNIVERSITY OF TECHNOLOGY